

WHITE DWARFS IN THE UKIRT INFRARED DEEP SKY SURVEY DATA RELEASE 9

P.-E. Tremblay^{1,2}, S. K. Leggett³, N. Lodieu^{4,5}, B. Freytag⁶, P. Bergeron⁷, J. S. Kalirai¹, and
H.-G. Ludwig⁸

¹*Space Telescope Science Institute, 700 San Martin Drive, Baltimore, MD, 21218, USA*

²*Hubble Fellow*

tremblay@stsci.edu

³*Gemini Observatory, Northern Operations Center, 670 North A'ohoku Place, Hilo, HI, 96720, USA*

⁴*Instituto de Astrofísica de Canarias (IAC), C/ Vía Láctea s/n, E-38200 La Laguna, Tenerife, Spain*

⁵*Departamento de Astrofísica, Universidad de La Laguna (ULL), E-38205 La Laguna, Tenerife, Spain*

⁶*Astronomical Observatory, Uppsala University, Regementsvägen 1, Box 515, SE-75120 Uppsala, Sweden*

⁷*Département de Physique, Université de Montréal, C. P. 6128, Succursale Centre-Ville, Montréal, QC H3C 3J7, Canada*

and

⁸*Zentrum für Astronomie der Universität Heidelberg, Landessternwarte, Königstuhl 12, Heidelberg, 69117, Germany*

ABSTRACT

We have identified eight to ten new cool white dwarfs from the Large Area Survey (LAS) Data Release 9 of the United Kingdom InfraRed Telescope (UKIRT) Infrared Deep Sky Survey (UKIDSS). The data set was paired with the Sloan Digital Sky Survey (SDSS) to obtain proper motions and a broad *ugrizYJHK* wavelength coverage. Optical spectroscopic observations were secured at Gemini Observatory and confirm the degenerate status for eight of our targets. The final sample includes two additional white dwarf candidates with no spectroscopic observations. We rely on improved 1D model atmospheres and new multi-dimensional simulations with CO5BOLD to review the stellar parameters of the published LAS white dwarf sample along with our additional discoveries. Most of the new objects possess very cool atmospheres with effective

temperatures below 5000 K, including two pure-hydrogen remnants with a cooling age between 8.5 and 9.0 Gyr, and tangential velocities in the range $40 \text{ km s}^{-1} \leq v_{\text{tan}} \leq 60 \text{ km s}^{-1}$. They are likely thick disk 10-11 Gyr-old objects. In addition we find a resolved double degenerate system with $v_{\text{tan}} \sim 155 \text{ km s}^{-1}$ and a cooling age between 3.0 and 5.0 Gyr. These white dwarfs could be disk remnants with a very high velocity or former halo G stars. We also compare the LAS sample with earlier studies of very cool degenerates and observe a similar deficit of helium-dominated atmospheres in the range $5000 < T_{\text{eff}} \text{ (K)} < 6000$. We review the possible explanations for the spectral evolution from helium-dominated towards hydrogen-rich atmospheres at low temperatures.

Subject headings: white dwarfs – stars: fundamental properties – infrared: stars – techniques: photometric – techniques: spectroscopic – surveys

1. INTRODUCTION

The remnants of most intermediate mass stars ($0.6 \lesssim M/M_{\odot} \lesssim 8$) are C/O core white dwarfs with a hydrogen or helium-rich atmosphere. The cooling rate of white dwarfs decreases as they age and the oldest remnants in the solar neighborhood have atmospheres that are warmer than most stars in the same environment. Due to their small radius, however, cool degenerate stars are intrinsically faint and the local sample is only complete **out** to about 20 pc (Holberg et al. 2008; Sion et al. 2009; Giammichele et al. 2012). Early studies of the white dwarf local population have shown that the observed luminosity function drops off for effective temperatures $T_{\text{eff}} \lesssim 4000 \text{ K}$, and corresponding ages in the range of 8-10 Gyr, which is consistent with the formation time of the Galactic thin disk (Winget et al. 1987; Liebert et al. 1988; Leggett et al. 1998).

Cool white dwarfs are unambiguously old since their time on the cooling sequence is a significant fraction of the galactic age. Given that the mass of a remnant is known, it is possible to derive the initial mass of the star and the total age of the white dwarf by using the initial-final mass relation calibrated from clusters (see, e.g., Kalirai et al. 2008; Williams et al. 2009; Dobbie et al. 2012). However, spectroscopic observations of very cool white dwarfs, with $T_{\text{eff}} \lesssim 5000 \text{ K}$ depending on the resolution, show no hydrogen or helium lines (DC spectral type) that can be used to constrain the surface gravity. Furthermore, photometric information is not sufficient to constrain masses unless trigonometric parallax observations are available (Bergeron et al. 1997). In order to identify thick disk or halo white dwarfs in the solar neighborhood, recent studies have instead relied on photometry coupled with kinematics (Kilic et al. 2009, 2010; Lodieu et al. 2009; Leggett et al. 2011). They also secured spectroscopic observations for most targets to confirm the degenerate nature. Remnants that have halo or thick disk kinematics, along with large cooling ages assuming a typical gravity of $\log g = 8$, are then selected as likely candidates for those galactic components. Follow-up parallax observations can confirm the membership of these candidates by providing masses and, hence, total ages (see, e.g., Kilic et al. 2012). It is hoped that kinematic, photometric, and parallax data

from the *Gaia* survey will identify a significant halo and thick disk population **of white dwarfs** (Carrasco et al. 2014).

In order to exploit the full potential of future surveys to study old galactic populations, the accuracy of the cool white dwarf models must be improved. One of the most pressing issues is to solve the discrepancy between the observed and predicted collision-induced absorption (CIA) features due to H_2 molecules. The current model fits of cool degenerates with a derived pure-hydrogen atmosphere and $T_{\text{eff}} \lesssim 4000$ K, or a mixed helium-hydrogen (He/H) atmosphere below $T_{\text{eff}} \sim 6000$ K, are not fully satisfactory (Bergeron & Leggett 2002; Kilic et al. 2008; Leggett et al. 2011; Kilic et al. 2012), although it is hoped that improved CIA opacity calculations (see, e.g., Frommhold et al. 2010) will solve this issue.

Another uncertain aspect is related to the chemical evolution of cool white dwarfs. Kowalski & Saumon (2006) have found the previously missing Lyman α ($\text{Ly}\alpha$) red wing opacity which has a strong impact on the blue part of the visible flux (e.g. SDSS u and g bands) of cool H-rich atmospheres ($T_{\text{eff}} \lesssim 5500$ K). Recent studies that have relied on this opacity (Kilic et al. 2010; Giammichele et al. 2012) suggest that most DCs below $T_{\text{eff}} < 5000$ K appear to have H-rich atmospheres. On the other hand, analyses without the $\text{Ly}\alpha$ opacity (Bergeron et al. 2001; Kilic et al. 2009; Leggett et al. 2011) derive a ratio of helium to hydrogen atmospheres that is roughly 50% in the same T_{eff} range, similar to what is observed at warmer temperatures ($6000 < T_{\text{eff}}$ (K) < 8000 ; Tremblay & Bergeron 2008; Giammichele et al. 2012). There is currently no physical model able to explain the spectral evolution towards H-rich atmospheres suggested by the photometric analyses including the $\text{Ly}\alpha$ opacity. It is important to understand the properties of this chemical evolution since the **derived age estimates** of cool remnants can change by ~ 1 Gyr depending on the total amount of hydrogen present in the white dwarf (Fontaine et al. 2001).

In this work, we use the United Kingdom InfraRed Telescope (UKIRT) Infrared Deep Sky Survey (UKIDSS; Lawrence et al. 2007) Large Area Survey (LAS) Data Release (DR) 9 coupled with the Sloan Digital Sky Survey (SDSS; York et al. 2000) to identify 18 white dwarf candidates, out of which eight are confirmed as degenerates from spectroscopy. We also identify two more possible white dwarfs without spectroscopic confirmation. We combine them with the white dwarfs identified in previous LAS data releases (Lodieu et al. 2009; Leggett et al. 2011, thereafter Paper I and Paper II, respectively) to form a sample of 30 cool white dwarfs. We review the properties of this sample, in particular the chemical abundances, by employing improved 1D model atmospheres including the $\text{Ly}\alpha$ red-wing opacity. On the theoretical side, we also present the first 3D model atmospheres of very cool pure-H white dwarfs in order to estimate the 3D effects on the predicted spectra. These hydrodynamical simulations may be the first step in understanding the chemical evolution of cool white dwarfs, which could be caused by events related to convection in the deeper layers that are not currently part of our 3D simulations.

We begin in Section 2 by presenting an overview of the LAS sample of cool white dwarfs from Paper I and II as well as the white dwarf candidates observed photometrically and spectroscopically

in this work. Section 3 describes our 1D and new 3D model atmospheres employed to study these former stars. We continue in Section 4 by comparing the objects in the LAS sample to model predictions in order to determine updated stellar properties. We review the status of the spectral evolution of cool white dwarfs in Section 5 and conclude in Section 6.

2. SAMPLE SELECTION AND OBSERVATIONS

The study presented here involves the white dwarfs identified from the pairing of the UKIDSS LAS and SDSS surveys in Paper I and II. We begin with a brief review of the sample selection and observations in the published sample, and then we present new candidate white dwarfs identified from the LAS DR9.

2.1. UKIDSS LAS Sample

The LAS is a sub-survey of UKIDSS aimed at identifying cool and faint galactic sources in the $YJHK$ bands (Hewett et al. 2006) with a large photometric depth. In Paper I, target white dwarfs were selected in the 280 deg^2 sky area of the LAS DR2, producing a sample of seven new white dwarfs with $T_{\text{eff}} \sim 6000 \text{ K}$, confirmed with optical spectroscopy obtained at Gemini Observatory. Paper II used the larger 1400 deg^2 area covered by the LAS DR6 and refined the color selection to identify 13 more white dwarfs, including seven objects with $T_{\text{eff}} < 4500 \text{ K}$.

Near-infrared photometry is essential to characterize cool white dwarfs since the CIA due to H_2 molecules is observed in this wavelength range. It is also crucial to have a broad wavelength coverage in order to determine precise T_{eff} values. The LAS and SDSS databases were therefore cross-correlated in order to add $ugriz$ photometric information. Furthermore, proper motions were derived using the target coordinates and the epochs of the SDSS and UKIDSS images. Sources were matched by requiring the presence of a primary SDSS source within $5''$ of one LAS point source coordinate.

The color and reduced proper motion (RPM) selection of the published LAS white dwarf candidates is discussed in Paper I (Section 3) and II (Section 2.3). In brief, the search was restricted to high proper-motion sources with RPM values of $H_g = g + (5 \log(\mu) + 5) > 20.5$ (20.35 in Paper I), where g is the SDSS magnitude and μ the proper motion. The near-infrared flux was limited to $14 \leq J \leq 19.6$ to ensure non-saturation and a good detection while the restriction $r_{\text{AB}} < 20.7$ was employed to allow for spectroscopic observations of the candidates. In Figures 1 and 2 we present the sample of Paper I and II in the H_g vs. $g - i$ RPM diagram, and $r - i$ vs. $g - r$ and $J - H$ vs. $i - J$ color versus color diagrams, respectively.

In Paper I, sources as faint as 19.7 in H were selected, although it was found that LAS uncertainties were significantly underestimated for such large H magnitudes. In particular, many

of the objects selected as probable very cool white dwarfs with $J - H < -0.1$ were in fact warmer degenerates with hydrogen-line spectra (DA) that were scattered into the color selection because H was too faint. This led to a more stringent color selection and the acquisition of repeat JHK photometry, using the WFCAM on UKIRT and NIRI on Gemini North, for most candidates in Paper II. It was confirmed that for $H \gtrsim 18$, LAS H -band magnitudes are too faint by about 2σ .

We updated the photometry presented in Paper I and II by relying on the improved data reduction from the Data Release 10 of both the SDSS and LAS surveys. We employ this improved data set to derive updated atmospheric parameters in Section 4.

2.2. New White Dwarf Candidates

In this work, we have employed the LAS DR9 combined with the SDSS DR9 (Ahn et al. 2012) to identify 18 new cool white dwarf candidates. The LAS DR9 covers 3176 deg^2 , most of which is also covered in SDSS DR9 since UKIDSS was originally designed to provide a near-infrared counterpart to the SDSS survey. This suggests that we can significantly enhance the size of the sample compared to the earlier studies. We refer to Paper II for a review of the derivation of the proper motions from the combined SDSS/LAS data.

Table 1 gives the astrometric information for the new candidates, and Table 2 presents the observed photometry and associated uncertainties. While the sample was identified and selected from the SDSS and LAS DR9, the photometric and astrometric data used for our analysis and presented in Tables 1 and 2 is drawn from the DR10 of both surveys. It was found that the new SDSS/LAS astrometry implies much smaller proper motions for four objects, which led us to discard J0349–00 and J0838+24 since they are likely to be G- to K-type (sub)dwarfs ($H_g < 20$).

Table 1 identifies the three different RPM and color regions where white dwarf candidates were selected in this work. Region A corresponds to cool $T_{\text{eff}} \sim 4000 \text{ K}$ pure-H atmospheres, and this is where most white dwarfs were detected in earlier studies. Out of ten candidates in this area, eight were confirmed spectroscopically as white dwarfs (see Section 2.3), one is a likely white dwarf with no spectrum, and one was found to be a G- to K-type (sub)dwarf. Region B aims at recovering mixed H/He objects with near-infrared CIA absorption, and we **extend** this search area compared to Paper II. This selection did not result in any new confirmed white dwarf as all four candidates with $H_g > 20$ were found to be either subdwarfs or extragalactic sources. We also created a third search **criterion** to identify objects with no H or K detection although it only resulted in one more object (J0916+30) as a likely white dwarf, while one other was confirmed as a main-sequence star. As also concluded in Paper II, the region A selection robustly identifies white dwarfs with $T_{\text{eff}} = 4100\text{--}4700 \text{ K}$, and cooling ages of 7–9 Gyr.

Two of our candidates, J1240+25E and J1240+25W, have a close projected position on the sky. Over the period of 5.12 years covered between the SDSS DR10 and UKIDSS DR10 detections, the East component shows a proper motion of $+1''.338$ in

RA and $+0''.103$ in Dec. Over this same period the West component moves $+1''.348$ in RA and $+0''.120$ in Dec. Given the close projected proximity, the movement in the same direction across the sky, and the agreement in the measured motion to within 4 mas yr^{-1} , we can identify the pair as a binary.

2.3. Additional Observations

We obtained additional near-infrared photometry for a subset of the sample where LAS data were missing. Repeat photometry was also secured for objects where LAS uncertainties are larger than $\sim 0.1 \text{ mag}$ since the errors are likely to be underestimated in those cases (see Paper II). The additional YJHK photometry was obtained for 12 targets using NIRI (Hodapp et al. 2003) on Gemini North. In Table 3 we present the observation log and the data are given in Table 4.

Optical spectroscopic observations were obtained for 13 objects and eight of them turned out to be genuine white dwarfs. The Gemini Multi-Object Spectrographs (GMOS; Hook et al. 2004) at both Gemini North and South were used for all new observations. The R400 grating was employed with the GG455 blocking filter and the central wavelength was 680 nm, with wavelength coverage of 460-890 nm. As in Paper II, the $0.''75$ slit was used with 2×2 binning and the resulting resolution is $R \sim 1280$ or 5.5 \AA .

Figure 3 shows the GMOS spectra of the new white dwarfs. All of them are featureless and consistent with the DC classification except for J1240+25E which shows a weak pressure-broadened $H\alpha$. In the following we add two objects without spectra in our sample (J0100+11 and J0916+30) since the photometric fits and tangential velocities suggest they could be white dwarfs (see Section 4.2). We also rely on the white dwarf spectra presented in Paper I and II for objects found in earlier LAS data releases.

The eight new spectroscopically confirmed white dwarfs and two degenerate candidates are presented in the RPM and color vs. color diagrams of Figures 1 and 2 along with white dwarfs discovered in earlier LAS data releases. We also illustrate the search regions A, B, and C. There is a significant number of new objects outside of the search regions since we rely on the updated DR10 samples and NIRI photometry instead of the DR9 used in the initial selection. **As in our earlier studies, some objects were scattered into the color selection because LAS H was too faint.**

3. MODEL ATMOSPHERES

3.1. 1D Atmospheres

We rely on pure-H, pure-He, and mixed composition 1D model atmospheres that are similar to those described and used in Paper I, Paper II, Kilic et al. (2010), Giammichele et al. (2012), and Catalán et al. (2012). Contrary to earlier studies of LAS white dwarfs, the pure-H models now include the Ly α red wing opacity from Kowalski & Saumon (2006), while the pure-He and mixed composition models are identical to those described in Kilic et al. (2010). The mixed composition atmospheres have ratios of He to H by number ranging from values of 10^{-2} to high values of 10^{10} . All models rely on the mixing-length theory (MLT; under the $ML2/\alpha = 0.8$ parameterization) to treat convective energy transfer.

3.2. Multi-Dimensional Effects

For the coolest DA white dwarfs, there is no change in the predicted spectra when the mixing-length parameterization of the MLT is varied in the model atmospheres (Bergeron et al. 1995). The source of this behavior is that the MLT predicts that convection is essentially adiabatic throughout the atmosphere (i.e. there is no significant entropy jump), in which case the thermodynamic structure only depends on the value of the adiabatic gradient and not on the properties of convective granules, such as the horizontal extent and lifetime.

It is desirable to confirm the robustness of the 1D approximation for cool white dwarfs. For that purpose, we have computed CO⁵BOLD multi-dimensional simulations for $T_{\text{eff}} = 3770$ and 4520 K, in both cases at $\log g = 8$. We present the properties of these simulations in Table 5. The **2D** models use the same numerical setup as the one described in Tremblay et al. (2013a) where the coolest simulations are at $T_{\text{eff}} = 6000$ K. **On the other hand, the 3D simulations rely on a new version of CO⁵BOLD with advances for low-Mach-number flows (Freytag 2013). The improved numerical schemes are less diffusive and provide proper granulation in brown dwarfs (i.e. similar to models at higher Mach numbers).** In brief, we rely on an **equation of state** and opacities that are the same as those of our 1D model atmospheres described above. We employ an 8 opacity bin scheme to describe the band-integrated radiative transfer. The wavelength dependent opacities are sorted based on the Rosseland optical depth (τ_R) at which $\tau_\lambda = 1$ and we take $150 \times 150 \times 150$ grid points to solve the radiative transfer and hydrodynamical equations. We have derived T_{eff} from the temporally and spatially averaged emergent stellar flux.

Figure 4 demonstrates that the convective turnover timescale is rather similar in very cool DC white dwarfs and hotter DAs, with a value below one second. On the other hand, the radiative relaxation timescale is more than 30 seconds in all layers at $T_{\text{eff}} = 4520$ K which is rather long compared to DAs. It implies that radiative transfer will have little impact on the structure of the convectively unstable layers. This decoupling between the two timescales is also unfortunate for 3D

simulations, since one must use small time steps to solve the dynamical equations and have a long total time to cover the radiative relaxation time. This problem is similar to the one encountered in Tremblay et al. (2013a, see Section 3.3) for cool DA white dwarfs ($T_{\text{eff}} \lesssim 8000$ K). As in Tremblay et al. we perform instead non-gray 2D simulations where it is possible to cover a few radiative relaxation timescales. Tremblay et al. (2013a) have shown that most of the multi-D effects are already in the 2D simulations, and that 3D mean structures are only slightly different to their 2D counterparts.

We find that both our models at $T_{\text{eff}} = 3770$ and 4520 K reach an almost completely adiabatic structure in all layers. This outcome is similar to the coolest DA models in Tremblay et al. (2013a). The convective overshoot causes the entropy gradient in the upper layers to relax to an adiabatic structure even in regions that are stable to convection in 1D. In Figure 5, we compare 1D and $\langle 2D \rangle$ structures for the simulation at 3770 K. The spatial and temporal averages are performed over surfaces of constant Rosseland optical depth and for 12 random snapshots. We observe that both structures are nearly identical, except for the very top layers. The results are very similar for the 4520 K case. In these cool objects, H_2 molecule formation causes a strong collision-induced absorption, and even the 1D model atmospheres are unstable to convection up to $\tau_{\text{R}} \sim 10^{-3}$. In the convective layers, the structure is adiabatic and identical for 1D and 2D models since they rely on the same equation of state. Therefore, we conclude that 1D model atmospheres relying on the MLT are appropriate to model current observations of cool DC white dwarfs.

3.3. 3D Granulation Properties

We have used our 2D simulations as initial conditions to compute 3D atmospheres for 10 seconds in stellar time. Since radiative relaxation timescales are much longer, we expect that the mean structure will remain adiabatic and there is little interest in using the mean properties of the 3D simulations. However, the 3D simulations allow the study of the granulation properties, which is impossible in 1D and rather limited in 2D.

Cool DC white dwarfs reach photospheric densities that are seen otherwise in cool M dwarfs and brown dwarfs. However, the latter objects contain metals in their atmospheres and are subject to molecule, grain, and cloud formation in and above their photosphere (Freytag et al. 2010). In Figure 6, we present intensity snapshots for our 3D simulations. The relative intensity contrast (see Eq. 73 of Freytag et al. 2012) is given on the top of each snapshot in Figure 6. For our coolest simulation at $T_{\text{eff}} = 3770$ K, the intensity contrast is remarkably small at 0.03%, although it is following the trend observed in Tremblay et al. (2013b) given the low Mach number value in Table 5. In the same table we also give the characteristic horizontal size of the granulation, which is roughly a factor of three **to four times** the pressure scale height at $\tau_{\text{R}} = 1$, in very good agreement with the trend found for cool DA white dwarfs where the characteristic size reaches a plateau at around **that value** for photospheric densities larger than $\sim 10^{-5} \text{ g cm}^{-3}$.

4. ANALYSIS AND RESULTS

4.1. Fitting Method

In order to determine the atmospheric parameters of our observed targets, we have first converted the magnitudes into observed fluxes using the method of Holberg & Bergeron (2006) and the appropriate filters. The SDSS magnitudes are converted to the AB system employing the u , i , and z corrections given in Eisenstein et al. (2006, see their Section 2). We fit the resulting energy distributions with those derived from model spectra, integrated over the same filters, using a non-linear least-squares method (Bergeron et al. 2001). Given our result that 3D effects are negligible, in the following we rely only on the 1D spectra described in Section 3.

From the fit of the observed energy distribution we constrain T_{eff} and the solid angle $\pi(R/D)^2$ where R is the radius of the star and D is its distance from Earth. Since predicted energy distributions depend only weakly on gravity and no parallax measurements are available, it is not possible to constrain the gravity of our objects. We therefore assume a surface gravity of $\log g = 8$. Most white dwarfs are found in a rather narrow range of gravity (Bergeron et al. 1992; Kleinman et al. 2013) and we employ, as in Paper II, a gravity uncertainty of ± 0.3 dex. The photometric variance uncertainties are obtained from the covariance matrix of the fit.

We rely on the mass-radius relation from the evolutionary models of Fontaine et al. (2001) with carbon-oxygen cores (50/50 by mass fraction mixed uniformly) to determine the radius, mass, and cooling age. We assume thick H layers ($M_{\text{H}}/M_{\text{total}} = 10^{-4}$) for H-atmosphere white dwarfs and thin layers ($M_{\text{H}}/M_{\text{total}} = 10^{-10}$) for He and mixed atmospheres. We also derive the distance to our targets by combining the mass-radius relation and the best-fit solid angle. The $\log g = 8.0 \pm 0.3$ assumption dominates the uncertainties on our derived masses and cooling ages. On the other hand, it has little impact on the T_{eff} determinations for which the uncertainty is dominated by the photometric variance. Compared to Paper II, we include the SDSS u and g filters for all fits since our model spectra rely on the Ly α red wing opacity. We use NIRI instead of LAS near-infrared photometry when available, and neglect LAS photometry with uncertainties larger than 0.15 mag since it was found in earlier studies that errors were significantly underestimated in those cases.

Finally, the surface composition is constrained from both the optical spectra at H α and the photometry. Since H α absorption is not seen in H-rich white dwarfs cooler than ~ 5000 K, we can only rely on the photometric fit in those cases. When possible, we also estimate effective temperatures from a fit of the H α equivalent width ($T_{\text{H}\alpha}$).

4.2. Stellar Parameters

The best-fit atmospheric parameters for the ten new white dwarfs drawn from the LAS DR9 and the 20 white dwarfs identified in Paper I and II are given in Table 6. We also derive distances and cooling ages from evolutionary models as discussed in Section 4.1. The distances and proper

motions, given in Table 1, are then used to compute the tangential velocity v_{tan} .

Among the newly identified white dwarfs, the fits shown in Figure 7 for the resolved binary ULAS J1240+25E/W are particularly interesting since we can compare the derived distance and age of both components. J1240+25E is clearly H-rich given the $\text{H}\alpha$ observation. However, while the photometric fit gives a temperature of ~ 5570 K, the equivalent width of $\text{H}\alpha$ is consistent with a ~ 300 K lower T_{eff} value, which is significantly larger than the variance allowed by the photometric uncertainties. The photometric and $T_{\text{H}\alpha}$ temperatures can be **brought into** agreement if the mass is very large ($> 1 M_{\odot}$). The other component, J1240+25W, does not show a clear $\text{H}\alpha$ absorption feature, and it is either a cooler H atmosphere or a He-rich object. The fit quality is average for both the pure-H (filled circles) and pure-He (open circles) cases, hence it is difficult to constrain the composition only from the photometric fit. However, the $u - g$ color has a large positive value, which is consistent with a $\text{Ly}\alpha$ red wing absorption. We therefore select the pure-H composition, also noticing that the spectrum shows a hint of a faint $\text{H}\alpha$ line. The cooling age of the system is 3.0 and 5.0 Gyr based on the East and West component, respectively. We look at this apparent discrepancy and compare the parameters of both components of the system under different assumptions in Section 4.3. Nevertheless, it is clear that both white dwarfs have a relatively low cooling age, and have a large velocity of $v_{\text{tan}} \sim 155 \text{ km s}^{-1}$, which could suggest disk remnants with a very high velocity or former halo G stars.

Figure 8 displays four new white dwarfs that are best fit with pure-H atmospheres. For J0815+24 and J2206+02, the cooling ages of 8.5-9.0 Gyr and the tangential velocities in the range $40 \text{ km s}^{-1} \leq v_{\text{tan}} \leq 60 \text{ km s}^{-1}$ suggest they are thick disk stars with a total age of 10-11 Gyr. Figure 9 exhibits two more new white dwarfs for which we could not constrain the composition based on the photometric fits and featureless DC spectra (J0024–00 and J2330+05). Finally, Figure 10 shows two objects for which we do not have spectra to confirm **their** degenerate nature. J0100+11 has a similar temperature to the coolest pure-hydrogen objects in our sample in Figure 8, but a significantly larger near-infrared flux that is better fitted with a pure-He model. This would be one of **the** coolest known white **dwarfs** with a derived pure-He composition if the nature of this object is confirmed.

We have also performed a new analysis of the 20 LAS white dwarfs from **Papers I and II**, with the main difference being that the pure-H models now include the $\text{Ly}\alpha$ red wing absorption. Furthermore, we rely on the more recently released SDSS and LAS DR10 photometry. The derived atmospheric parameters are similar to those presented in earlier works. This is in part because the u and g observations were not included in the fitting procedure in earlier studies. We show three examples of cool pure-H degenerates in Figure 11 where the fit in the blue region is very good for the pure-H solution, even though there is only a moderate change in the atmospheric parameters compared to Paper II.

The fits for pure-He and mixed objects are very similar to those of Paper I and Paper II. However, it was necessary to review the composition assigned to the DC white dwarfs because of

the improved pure-H fits. Recent studies relying on the Ly α red wing opacity have found that most DC white dwarfs below $T_{\text{eff}} \sim 5000$ K have a H-rich atmosphere (Kowalski & Saumon 2006; Kilic et al. 2009; Giammichele et al. 2012). In Figure 12, we present the observed $r - i$ vs. $u - g$ color vs. color diagram for our sample compared with theoretical sequences for pure-H and pure-He atmospheres. The observed scatter is relatively large, although this may be due to a scatter in the unknown surface gravities. We remark that most objects identified as pure-He white dwarfs in Paper I and Paper II (blue filled circles) actually follow the pure-He sequence (blue dashed lines) in Figure 12 and show no significant blue absorption. Hence, even by adding the blue filters neglected in previous works, this does not impact the derived composition for the three cool pure-He DC white dwarfs J1006+09, J1206+03, and J1351+12. However, we have updated the pure-He classification for J1454–01, which is now unconstrained since the pure-H fit is comparable to the pure-He fit, both shown in Figure 10. Furthermore, J0121–00, which previously had an unconstrained composition, is now better fit with a pure-hydrogen atmosphere (displayed in Figure 11 and with a black triangle in Figure 12).

We have derived T_{eff} values based on the equivalent width of the H α line, when observed, that can be compared with the photometric results. Since the strength of H α depends on the unknown gravities, our values should be considered as estimates only. For most of the DAs observed in Paper I, $T_{\text{H}\alpha}$ is significantly lower than the photometric temperature. We note that only *ugrizYJ* was used in the photometric fit since the faint LAS *H* for those objects was found to be unreliable. One explanation is that the objects could be very massive white dwarfs, which would explain a weaker H α . Alternatively, it is possible that even the uncertainties for the *ugrizYJ* photometry have been underestimated. We note that some of the objects with LAS photometry, such as J0226–00, J1323+12, and J1522+08, reveal a good agreement between photometric and H α temperatures.

4.3. J1240+25E/W Binary System

In this section, we compare the stellar parameters of the two cool white dwarfs found in the resolved double degenerate system J1240+25E/W. The objective is to better constrain the properties of the system considering the fact that the total age and distance should be the same for both objects. We have attempted to vary the gravity of the components in order to match both the total ages and distances. To compute the total age, we use the initial-final mass relation of Kalirai et al. (2008) with a third order polynomial fit, and the main-sequence lifetimes of Hurley et al. (2000). We reject solutions for which the total age is larger than 13 Gyr. We only consider the photometric variance in the uncertainties, hence we neglect the effects of varying the initial-final mass relation. We therefore consider that an agreement at the 3σ level is acceptable.

In Figure 13, we display the log g couples for which both total ages and distances are in agreement. Different combinations are shown in terms of the uncertain T_{eff} value of J1240+25E and composition of J1240+25W. The photometric T_{eff} solution for J1240+25E and pure-H composition for J1240+25W (top-left panel) do not allow the ages and distances to both match within

1σ (black) although there are possible solutions within 2σ (blue) or 3σ (cyan). The bottom-left panel demonstrates that when relying on the spectroscopic T_{eff} for J1240+25E, the agreement is much better, and multiple solutions are possible including the $\log g \sim 8$ canonical value for both components. The pure-He solution for J1240+25W also provides matching ages and distances, although only for higher gravities. Our results do not provide strong constraints on the composition or atmospheric parameters, but demonstrate that the apparent age discrepancy assuming $\log g = 8$ can be resolved if we allow the gravities to vary. Parallax measurements for the system will be necessary to determine the distance and total age. The analysis also suggests that the spectroscopic solution for J1240+25E is preferred, and that underestimated photometric uncertainties are causing the discrepancy between the spectroscopic and photometric T_{eff} solutions. We notice from Figure 7 that the shape of the energy distributions between i and Y are fairly different between the observations and predictions. **Since the problem is not generally observed in other data sets (see, e.g., Bergeron et al. 2001), it is likely an issue with the observations.**

5. CHEMICAL EVOLUTION

5.1. Observational Status

In view of our results and those of similar recent studies, we review the status of the spectral evolution of white dwarf atmospheres below $T_{\text{eff}} \sim 6000$ K. In order to have all studies on an equal footing, we have refitted the *ugrizJHK* photometry for the 126 cool white dwarfs in Kilic et al. (2010) with models including the $\text{Ly}\alpha$ opacity. In Figure 14, we compare the observed $u - g$ colors for their sample with predictions from model atmospheres. Most objects with a pure-He composition assigned in Kilic et al. (2010) are actually in better agreement with the new pure-H sequence. However, most of the pure-He objects are relatively warm ($T_{\text{eff}} > 4600$ K) and in a regime where the predicted differences between the pure-H and pure-He colors are close to the photometric uncertainties. We have inspected the individual fits (not shown here), and the new pure-H fits do not always provide an obvious better match to the observations. We refrain from assigning new compositions to the objects for the time being, although Figure 14 demonstrates that it is a likely possibility that most derived pure-He atmospheres with $T_{\text{eff}} < 5000$ K in Kilic et al. (2010) are actually H-rich atmospheres. In the following we consider both possibilities.

In Table 7, we present the fraction of He-dominated atmospheres ($N_{\text{He-dom}}/N_{\text{total}}$) found in this work, as well as in the similar studies of Giammichele et al. (2012), Kilic et al. (2009), and Kilic et al. (2010), respectively. We take the value of $\text{He}/\text{H} = 1$ in number as the break point between the two compositions in cases of mixed atmospheres. For the local sample of Giammichele et al. (2012), we only include objects within 20 pc, allowing for a nearly volume complete sample and a better representation of the local population.

The so-called non-DA gap in the range $5000 < T_{\text{eff}} \text{ (K)} < 6000$ was first discussed in Bergeron et al. (1997), where they found very few pure-He atmosphere white dwarfs in that temperature range. In

this regime, it is fairly straightforward to define the main constituent of the atmosphere, since the detection of $H\alpha$ and the agreement of its observed equivalent width with predictions using the photometric T_{eff} allows the confirmation of the pure-H interpretation. On average, recent studies from Table 7 suggest that only $\sim 25\%$ of the white dwarfs in that T_{eff} range possess He-dominated atmospheres. This confirms a deficit in He atmospheres since for slightly warmer objects ($6000 < T_{\text{eff}}$ (K) < 8000), the ratio is in the range 40-50% (Tremblay & Bergeron 2008; Giammichele et al. 2012).

It was understood early that He-atmospheres are found in the non-DA gap (see the discussion in Bergeron et al. 2001), although in most cases they are peculiar white dwarfs with pressure shifted C_2 bands (spectral type DQpec, see Kowalski 2010a) or metals (DZ). Furthermore, a significant fraction of cool He-dominated atmospheres have a derived mixed He/H composition due to the presence of near-infrared CIA H_2 -He absorption. Indeed, for the local white dwarf sample within 20 pc, Giammichele et al. (2012) find 25% of He-dominated atmospheres in the non-DA gap, and in the six identified He-atmospheres, four are DQpec stars. The LAS sample is smaller and does not allow for a statistically significant characterization of the He-rich population in the non-DA gap, although our results are in agreement with those of Giammichele et al. (2012), with a non-DA fraction of 25% and one of the two He-rich objects is a DQpec (SDSS J1247+06; Kilic et al. 2006). The survey of Kilic et al. (2010) is also in agreement with a non-DA gap, and more than half of the He-dominated atmospheres (with spectroscopic observations) are DQpec, DZs, or mixed He/H DCs with significant near-infrared absorption. Finally, the sample of Kilic et al. (2009) is drawn from Bergeron et al. (2001) and they did not include any of the DQpec stars. Therefore, we believe that their low He-atmosphere fraction is due to their target selection and we do not discuss further this sample.

The non-DA gap described in Bergeron et al. (2001) has a red edge at $T_{\text{eff}} \sim 5000$ K. It is however difficult to differentiate between pure-He and pure-H atmospheres at cooler temperatures since both compositions have the DC spectral type. We exclude objects with a derived T_{eff} below 4000 K since we lose the thin disk contribution in this range, and most ultracool objects have peculiar colors which are likely to lead to strong selection biases in magnitude limited samples.

Giammichele et al. (2012) find that $N_{\text{He-dom}}/N_{\text{total}} = 24\%$ in the range $4000 < T_{\text{eff}}$ (K) < 5000 when employing the $\text{Ly}\alpha$ opacity. All He-rich objects are DQpec, DZs, or mixed He/H DCs, hence they find a white dwarf population that is very similar to that found in the non-DA gap. This suggests that the non-DA gap is not actually a gap but a one-time chemical evolution near $T_{\text{eff}} \sim 6000$ K. The sample of Kilic et al. (2010) includes seven He-rich mixed DC white dwarfs and one DZA in the range $4000 < T_{\text{eff}}$ (K) < 5000 , which implies a minimum ratio of $N_{\text{He-dom}}/N_{\text{total}} = 14\%$ even if we consider that all derived pure-He atmospheres are actually H-rich. Based on our new fits with models including the $\text{Ly}\alpha$ opacity and the fact that the $u - g$ colors in Figure 14 show little evidence of pure-He compositions, it is unlikely that the number of He-dominated atmospheres is much larger than the minimum fraction. Our sample has a higher fraction of He-atmospheres in the same range, with a minimum of 18% based on the fraction of mixed objects, but a value of 46% if we include the three DC white dwarfs that are better fitted with pure-He models and if

we exclude unconstrained compositions. This result is certainly at **odds** with the other samples, although our sample is fairly small and the color selections favor the detection of mixed objects. It is also possible that the discrepancy described in Sections 4.2 and 4.3 between the observed photometry and predictions has an impact on the derived compositions at low T_{eff} . All in all, there is no clear evidence with the most recent models and observations, compared to the picture presented in Bergeron et al. (2001), that the number of He-dominated atmospheres increases below $T_{\text{eff}} = 5000$ K.

5.2. Theoretical Status

In the following, we review the possible explanations for the spectral evolution of He-atmospheres towards H-atmospheres at $T_{\text{eff}} \sim 6000$ K. First of all, it could be caused by events in the interior, perhaps in a way analogous to the convective mixing that is observed from DA to DB between 30,000 and 20,000 K and from DA to DC at around 8000 K (Bergeron et al. 2011; Tremblay & Bergeron 2008). The turnover timescales in white dwarf convective zones, even in the deepest layers, are less than a few hours (Van Grootel et al. 2012), hence many orders of magnitude shorter than the characteristic cooling times. It appears improbable that hydrogen could float on the surface due to incomplete mixing. However, if the microscopic diffusion timescale of hydrogen in the helium-rich plasma dominates over the turnover timescale somewhere within the convective zone, it might be possible to create an abundance gradient.

According to Tassoul et al. (1990), the convective zone in pure-He DC white dwarfs stops growing at $M_{\text{He}}/M_{\text{tot}} \sim 10^{-6}$ once it reaches the degenerate core at around 10,000 K. In the highly degenerate parts, conduction becomes the dominant energy transfer mechanism, although convection is still predicted to take place in layers with a relatively high level of degeneracy. Below $T_{\text{eff}} \sim 10,000$ K, the size of the convective zone slowly decreases due to the growing degenerate core, although between 7000 and 5000 K, the total mass included in the convective zone only decreases by ~ 0.4 dex according to Table 4 of Fontaine & van Horn (1976). This slow evolution is in part because the level of degeneracy increases very slowly with depth for adiabatic convection (see Eq. 13 of Böhm 1968). It is therefore unlikely that changes in the composition of the atmosphere would be linked to changes in the size of the convective zone. We note that since the internal core is directly linked to the convective zone in that regime, chemical evolution will lead to a change in the relation between the surface and core temperatures. At a given initial T_{eff} , a He-atmosphere white dwarf turning to a H-atmosphere would result in an object with a slightly lower T_{eff} due to the larger difference between the core and atmospheric temperatures in a DA white dwarf (Chen & Hansen 2011). This has to be taken into account in a spectral evolution model.

Chen & Hansen (2012) put forward a scenario where a significant fraction of H-atmospheres turn into He-dominated atmospheres at $T_{\text{eff}} \sim 6000$ K, and the resulting DC objects are shifted to ~ 500 K higher T_{eff} by conservation of the core temperature. The larger cooling rates for the post-mixing objects would create a deficit of He-atmospheres below 6000 K. In their scenario,

He-atmospheres would still be found in large number at $T_{\text{eff}} < 5000$ K. We do not support this interpretation from the observational evidences presented here. Furthermore, there is no strong **constraint** on the total mass of hydrogen in DA white dwarfs to suggest a DA to DC transformation around 6000 K and $M_{\text{H}}/M_{\text{tot}} \sim 10^{-7}$. Instead we propose a DC to DA evolution from a yet unknown mechanism.

Finally, the transition could be caused by an external factor, such as the accretion of hydrogen from disrupted circumstellar material. Some relatively warm ($T_{\text{eff}} \sim 10,000$ K) He-dominated white dwarfs have already accreted a significant amount of hydrogen (see, e.g., Zuckerman et al. 2007). From an extrapolation of the accreted hydrogen masses from Jura et al. (2009) to cooler temperatures, very cool DC white dwarfs with a history of accretion may have hydrogen masses of the order of $M_{\text{H}}/M_{\text{tot}} \sim 10^{-8} - 10^{-6}$. The upper limit gives a mass of hydrogen similar to the mass of helium within the convective zone at $T_{\text{eff}} \sim 6000$ K. While this could be the explanation for the presence of mixed objects, this is insufficient to create a pure-hydrogen atmosphere, and especially it would be very difficult to explain a rather abrupt chemical evolution at $T_{\text{eff}} \sim 6000$ K, which corresponds to a cooling age of ~ 2 Gyr.

The difficulties in defining a theoretical scenario for the chemical evolution of very cool white dwarfs suggest that we may need to further define the observed populations in larger samples and identify the nature of the mixed, DQpec, and DZ degenerates as the first step.

6. CONCLUSION

The pairing of the LAS and SDSS samples, both from Data Release 9, revealed eight to ten new white dwarf candidates from a reduced-proper-motion and color selection. We have confirmed the degenerate status of eight objects from spectroscopic observations while two other objects without spectra could also be degenerate stars. Our comparison of the observations with model atmospheres suggests that most selected objects are very cool white dwarfs with $T_{\text{eff}} < 5000$ K. While we could not constrain the gravity from the photometry alone, we have taken into account gravity effects in our uncertainties. In three cases we could not constrain the composition but we have confirmed two very cool pure-hydrogen remnants with $T_{\text{eff}} \sim 4100$ K and cooling ages between 8.5 and 9.0 Gyr. The tangential velocities in the range $40 \text{ km s}^{-1} \leq v_{\text{tan}} \leq 60 \text{ km s}^{-1}$ suggest that they may be thick disk objects. We have also identified the resolved binary ULAS J1240+25E/W with two white dwarfs and an unusually large tangential velocity of $\sim 155 \text{ km s}^{-1}$. When relying on the spectroscopic $\text{H}\alpha$ temperature for J1240+25E, the total ages and distances agree for both components although an unique solution can not be found without an independent constraint on the gravities. The significantly hotter photometric temperature for J1240+25E suggests that there are still some unaccounted uncertainties in the SDSS and LAS photometric data at the faint end.

We have reviewed the properties of the published LAS white dwarf sample (Lodieu et al. 2009; Leggett et al. 2011) and updated two compositions given the predictions of improved model

atmospheres including the Ly α red wing opacity. We have also computed 2D and 3D simulations but have shown that the multi-dimensional effects are negligible for the predicted spectra. The full LAS sample of 30 objects has been used to study the spectral evolution from the number of helium- versus hydrogen-dominated atmospheres. We found that our results are similar to those of Kilic et al. (2010) and Giammichele et al. (2012) in the range $5000 < T_{\text{eff}} \text{ (K)} < 6000$ and we confirm a spectral evolution towards pure-H atmospheres around 6000 K. We have no theoretical explanation for this chemical evolution. We argue that the transition should be better defined from an observational point of view for a sample with a well known completeness at faint magnitudes.

We are grateful for P. Kowalski for providing us the Ly α broadening profiles. Support for this work was provided by NASA through Hubble Fellowship grant #HF-51329.01 awarded by the Space Telescope Science Institute, which is operated by the Association of Universities for Research in Astronomy, Inc., for NASA, under contract NAS 5-26555.

S.K. L. is supported by Gemini Observatory. N. L. was funded by the Ramón y Cajal fellowship number 08-303-01-02. N. L. is financially supported by the project AYA2010-19136 from the Spanish Ministry of Economy and Competitiveness (MINECO). This work was supported by Sonderforschungsbereich SFB 881 "The Milky Way System" (Subproject A4) of the German Research Foundation (DFG). This work is supported in part by the NSERC Canada and by the Fund FRQ-NT (Québec). J. K. was supported by the National Science Foundation (NSF) through grant AST-1211719.

Some of the data reported here were obtained as part of the United Kingdom Infrared Telescope (UKIRT) Service Programme; UKIRT is operated by the Joint Astronomy Centre on behalf of the Science and Technology Facilities Council of the U.K. This paper makes extensive use of the UKIRT Infrared Deep Sky Survey (UKIDSS); we are grateful to the WFCAM instrument team, the UKIRT staff, the UKIDSS team, the CASU data processing team, and the WSA group at Edinburgh.

This paper also makes use of Sloan Digital Sky Survey (SDSS) data. Funding for the SDSS and SDSS-II has been provided by the Alfred P. Sloan Foundation, the Participating Institutions, the National Science Foundation, the U.S. Department of Energy, the National Aeronautics and Space Administration, the Japanese Monbukagakusho, the Max Planck Society, and the Higher Education Funding Council for England.

This work is based on observations obtained at the Gemini Observatory, which is operated by the Association of Universities for Research in Astronomy, Inc., under a cooperative agreement with the NSF on behalf of the Gemini partnership: the National Science Foundation (United States), the Science and Technology Facilities Council (United Kingdom), the National Research Council (Canada), CONICYT (Chile), the Australian Research Council (Australia), Ministério da Ciência e Tecnologia (Brazil), and Ministerio de Ciencia, Tecnología e Innovación Productiva (Argentina).

REFERENCES

- Ahn, C. P., Alexandroff, R., Allende Prieto, C., et al. 2012, *ApJS*, 203, 21
- Bergeron, P., & Leggett, S. K. 2002, *ApJ*, 580, 1070
- Bergeron, P., Saffer, R. A., & Liebert, J. 1992, *ApJ*, 394, 228
- Bergeron, P., Wesemael, F., Lamontagne, R., et al. 1995, *ApJ*, 449, 258
- Bergeron, P., Ruiz, M. T., & Leggett, S. K. 1997, *ApJS*, 108, 339
- Bergeron, P., Leggett, S. K., & Ruiz, M. T. 2001, *ApJS*, 133, 413
- Bergeron, P., Wesemael, F., Dufour, P., et al. 2011, *ApJ*, 737, 28
- Böhm, K.-H. 1968, *Ap&SS*, 2, 375
- Catalán, S., Tremblay, P.-E., Pinfield, D. J., et al. 2012, *A&A*, 546, L3
- Carrasco, J. M., Catalán, S., Jordi, C., et al. 2014, *A&A*, 565, A11
- Chen, E. Y., & Hansen, B. M. S. 2011, *MNRAS*, 413, 2827
- Chen, E. Y., & Hansen, B. M. S. 2012, *ApJ*, 753, L16
- Dobbie, P. D., Day-Jones, A., Williams, K. A., et al. 2012, *MNRAS*, 423, 2815
- Eisenstein, D. J., Liebert, J., Harris, H. C., et al. 2006, *ApJS*, 167, 40
- Fontaine, G., & van Horn, H. M. 1976, *ApJS*, 31, 467
- Fontaine, G., Brassard, P., & Bergeron, P. 2001, *PASP*, 113, 409
- Freytag, B., Allard, F., Ludwig, H.-G., Homeier, D., & Steffen, M. 2010, *A&A*, 513, A19
- Freytag, B., Steffen, M., Ludwig, H.-G., et al. 2012, *Journal of Computational Physics*, 231, 919
- Freytag, B. 2013, *Memorie della Societa Astronomica Italiana Supplementi*, 24, 26
- Frommhold, L., Abel, M., Wang, F., Li, X., & Hunt, K. L. C. 2010, *American Institute of Physics Conference Series*, 1290, 219
- Fukugita, M., Ichikawa, T., Gunn, J. E., et al. 1996, *AJ*, 111, 1748
- Giammichele, N., Bergeron, P., & Dufour, P. 2012, *ApJS*, 199, 29
- Van Grootel, V., Dupret, M.-A., Fontaine, G., et al. 2012, *A&A*, 539, A87
- Hodapp, K. W., Jensen, J. B., Irwin, E. M., et al. 2003, *PASP*, 115, 1388

- Holberg, J. B., & Bergeron, P. 2006, *AJ*, 132, 1221
- Holberg, J. B., Sion, E. M., Oswalt, T., et al. 2008, *AJ*, 135, 1225
- Hewett, P. C., Warren, S. J., Leggett, S. K., & Hodgkin, S. T. 2006, *MNRAS*, 367, 454
- Hook, I. M., Jørgensen, I., Allington-Smith, J. R., et al. 2004, *PASP*, 116, 425
- Hurley, J. R., Pols, O. R., & Tout, C. A. 2000, *MNRAS*, 315, 543
- Jura, M., Muno, M. P., Farihi, J., & Zuckerman, B. 2009, *ApJ*, 699, 1473
- Kalirai, J. S., Hansen, B. M. S., Kelson, D. D., et al. 2008, *ApJ*, 676, 594
- Kilic, M., Munn, J. A., Harris, H. C., et al. 2006, *AJ*, 131, 582
- Kilic, M., Kowalski, P. M., Mullally, F., Reach, W. T., & von Hippel, T. 2008, *ApJ*, 678, 1298
- Kilic, M., Kowalski, P. M., Reach, W. T., & von Hippel, T. 2009, *ApJ*, 696, 2094
- Kilic, M., Leggett, S. K., Tremblay, P.-E., et al. 2010, *ApJS*, 190, 77
- Kilic, M., Thorstensen, J. R., Kowalski, P. M., & Andrews, J. 2012, *MNRAS*, 423, L132
- Kleinman, S. J., Kepler, S. O., Koester, D., et al. 2013, *ApJS*, 204, 5
- Kowalski, P. M. 2010a, *A&A*, 519, L8
- Kowalski, P. M., & Saumon, D. 2006, *ApJ*, 651, L137
- Lawrence, A., Warren, S. J., Almaini, O., et al. 2007, *MNRAS*, 379, 1599
- Leggett, S. K., Ruiz, M. T., & Bergeron, P. 1998, *ApJ*, 497, 294
- Leggett, S. K., Lodieu, N., Tremblay, P.-E., Bergeron, P., & Nitta, A. 2011, *ApJ*, 735, 62 (Paper II)
- Liebert, J., Dahn, C. C., & Monet, D. G. 1988, *ApJ*, 332, 891
- Lodieu, N., Leggett, S. K., Bergeron, P., & Nitta, A. 2009, *ApJ*, 692, 1506 (Paper I)
- Sion, E. M., Holberg, J. B., Oswalt, T. D., McCook, G. P., & Wasatonic, R. 2009, *AJ*, 138, 1681
- Tassoul, M., Fontaine, G., & Winget, D. E. 1990, *ApJS*, 72, 335
- Tokunaga, A. T., & Vacca, W. D. 2005, *PASP*, 117, 421
- Tremblay, P.-E., & Bergeron, P. 2008, *ApJ*, 672, 1144
- Tremblay, P.-E., Ludwig, H.-G., Steffen, M., & Freytag, B. 2013a, *A&A*, 552, A13

- Tremblay, P.-E., Ludwig, H.-G., Freytag, B., Steffen, M., & Caffau, E. 2013b, *A&A*, 557, A7
- Williams, K. A., Bolte, M., & Koester, D. 2009, *ApJ*, 693, 355
- Winget, D. E., Hansen, C. J., Liebert, J., et al. 1987, *ApJ*, 315, L77
- York, D. G., Adelman, J., Anderson, J. E., Jr., et al. 2000, *AJ*, 120, 1579
- Zuckerman, B., Koester, D., Melis, C., Hansen, B. M., & Jura, M. 2007, *ApJ*, 671, 872

Table 1. Astrometry for Candidate White Dwarfs

Short Name	Right Ascension HH:MM:SS.SS	Declination DD:MM:SS.S	Epoch Year	μ ''yr ⁻¹		RPM H_g	Search ^a Region
				RA	Dec		
ULAS J0024–00 ^b	00:24:39.96	–00:30:39.6	2001.8808	–0.051	–0.160	22.33	A
ULAS J0100+11 ^c	01:00:41.27	11:03:29.4	2008.8374	–0.093	0.071	20.99	A
SDSS J0113–02 ^{d,e}	01:13:55.25	–02:57:29.9	2001.8616	–0.05	0.39	24.64	B
SDSS J0130–04 ^{d,e}	01:30:21.48	–04:41:05.9	2008.9959	0.01	0.26	23.10	B
ULAS J0156–00 ^f	01:56:09.78	–00:14:50.4	2003.8863	–0.107	0.044	22.25	B
ULAS J0349–00 ^{c,g}	03:49:33.39	–00:21:11.1	2003.7384	–0.010	0.004	16.77	B
ULAS J0815+24 ^b	08:15:53.48	24:27:35.0	2003.0781	0.107	–0.059	21.49	A
ULAS J0838+24 ^{c,g}	08:38:36.19	24:03:05.6	2003.9712	–0.015	0.040	18.17	C
ULAS J0916+30 ^{c,g}	09:16:56.77	30:47:27.0	2004.1298	–0.046	0.057	20.14	C
ULAS J1240+25W ^b	12:40:29.26	25:59:48.1	2005.0479	–0.263	–0.023	23.08	A
ULAS J1240+25E ^b	12:40:29.48	25:59:47.6	2005.0479	–0.261	–0.020	22.54	A
ULAS J1409+07 ^b	14:09:44.24	07:43:55.3	2003.3219	–0.215	–0.062	21.60	A
ULAS J1607+26 ^b	16:07:38.95	26:08:47.2	2003.3247	0.046	0.156	21.44	A
ULAS J1640+28 ^{f,g}	16:40:26.38	28:11:52.1	2003.4068	–0.036	0.039	19.59	C
SDSS J2153+45 ^{d,f}	21:53:00.68	45:27:33.2	2006.4096	–0.23	0.23	23.78	B
ULAS J2206+02 ^b	22:06:23.88	02:24:47.1	2008.7527	–0.172	0.123	22.27	A
ULAS J2315–00 ^f	23:15:54.62	–00:13:32.8	2003.8863	0.025	0.069	20.93	A
ULAS J2330+05 ^b	23:30:22.55	05:40:22.2	2008.8156	0.136	–0.108	21.85	A

^aSearch queries are

- A: $H_g > 20.5$, $r < 20.7$, $H < 18.9$, $0.8 \leq g - r \leq 1.6$, $0.2 \leq r - i \leq 0.6$, $0.6 \leq i - J \leq 1.4$, $J - H \leq 0.2$
B: $H_g > 21.0$, $r < 21.0$, $J > 14.0$, $r - i \leq [(0.5g - r) - 0.4]$, $g - r \leq 2.0$, $r - i \leq 1.0$, $i - z \leq 0.5$, $\text{sdsstype}=6$
C: no H or K detection: $H_g > 20.5$, $r < 20.7$, $J \geq 19.0$, $y - j < 0.2$, $i - J < 1.0$, $r - i < 0.3$, $g - r < 1.2$

^bConfirmed as a white dwarf spectroscopically in this work.

^cNo optical spectrum

^dProper motion is determined from USNO catalog as specified in SDSS catalog

^eConfirmed as an extragalactic source spectroscopically in this work, implying incorrect proper motion.

^fConfirmed as a G- to K-type (sub)dwarf star spectroscopically in this work.

^gEarlier SDSS/UKIDSS astrometry implied larger proper motion.

Note. — The uncertainty in proper motion μ is ~ 14 mas yr⁻¹ (see Paper II).

Table 2. SDSS DR10 and UKIDSS LAS DR10 Photometry for Candidate White Dwarfs

Short Name	$u(\text{err})$	$g(\text{err})$	$r(\text{err})$	$i(\text{err})$	$z(\text{err})$	$Y(\text{err})$	$J(\text{err})$	$H(\text{err})$	$K(\text{err})$
ULAS J0024−00	22.76(0.34)	21.20(0.04)	20.14(0.02)	19.80(0.02)	19.57(0.06)	18.96(0.09)	18.71(0.13)	18.56(0.21)	...
ULAS J0100+11	23.49(0.63)	21.48(0.05)	20.65(0.04)	20.20(0.03)	20.16(0.12)	19.30(0.11)	18.84(0.10)	18.77(0.25)	...
SDSS J0113−02	25.11(0.88)	21.67(0.06)	20.43(0.03)	20.31(0.04)	20.57(0.16)
SDSS J0130−04	22.97(0.45)	21.02(0.04)	19.91(0.02)	19.79(0.02)	19.96(0.09)
ULAS J0156−00	24.12(0.57)	21.93(0.06)	21.06(0.04)	20.58(0.03)	20.19(0.10)	19.68(0.14)	19.07(0.15)
ULAS J0349−00	24.63(1.70)	21.61(0.13)	24.56(1.31)	24.22(1.33)	21.93(1.00)	19.80(0.12)	19.35(0.13)	19.20(0.18)	...
ULAS J0815+24	23.75(0.54)	21.05(0.03)	19.94(0.02)	19.53(0.02)	19.28(0.05)	18.76(0.05)	18.48(0.04)	18.63(0.21)	18.37(0.27)
ULAS J0838+24	21.00(0.07)	20.02(0.02)	19.88(0.02)	19.85(0.03)	19.94(0.08)	19.32(0.05)	19.16(0.08)
ULAS J0916+30	22.26(0.23)	20.82(0.03)	20.45(0.03)	20.35(0.04)	20.43(0.17)	19.67(0.07)	19.51(0.10)
ULAS J1240+25W	23.48(0.51)	20.98(0.03)	20.07(0.02)	19.76(0.02)	19.62(0.07)	19.00(0.06)	18.63(0.07)	18.71(0.13)	18.87(0.30)
ULAS J1240+25E	21.97(0.15)	20.44(0.02)	19.86(0.02)	19.62(0.02)	19.52(0.07)	18.80(0.05)	18.67(0.07)	18.35(0.09)	18.33(0.18)
ULAS J1409+07	21.80(0.14)	19.85(0.01)	18.99(0.01)	18.69(0.01)	18.51(0.03)	17.93(0.02)	17.59(0.03)	17.46(0.05)	17.40(0.12)
ULAS J1607+26	22.22(0.16)	20.38(0.02)	19.44(0.01)	19.04(0.01)	18.86(0.04)	18.31(0.05)	18.00(0.03)	17.89(0.08)	17.63(0.11)
ULAS J1640+28	22.51(0.38)	20.97(0.04)	20.62(0.04)	20.45(0.05)	20.84(0.29)	19.82(0.13)	19.73(0.22)
SDSS J2153+45	22.93(0.53)	21.22(0.05)	19.63(0.02)	19.28(0.02)	20.56(0.19)
ULAS J2206+02	22.32(0.30)	20.64(0.03)	19.51(0.02)	19.11(0.01)	18.83(0.04)	18.32(0.04)	17.99(0.05)	17.84(0.08)	17.93(0.13)
ULAS J2315−00	22.89(0.27)	21.60(0.05)	20.68(0.03)	20.17(0.03)	20.10(0.10)	19.31(0.08)	18.98(0.08)	18.87(0.18)	...
ULAS J2330+05	22.33(0.30)	20.65(0.03)	19.69(0.02)	19.26(0.02)	19.13(0.07)	18.62(0.05)	...	18.11(0.08)	18.24(0.18)

Note. — SDSS *ugriz* magnitudes are on the AB system (Fukugita et al. 1996). LAS *YJHK* are on the Mauna Kea Observatories (Vega) system (Tokunaga & Vacca 2005).

Table 3. Observation Log

Short Name	GMOS		NIRI	
	Date	Program	Date	Program
ULAS J0024–00 ^a			2012-07-10	GN-2012B-Q-109
ULAS J0100+11			2012-07-20	GN-2012B-Q-109
SDSS J0113–02	2011-07-09	GN-2011A-Q-98		
SDSS J0130–04	2011-07-26	GN-2011A-Q-98		
ULAS J0156–00	2012-08-28	GS-2012B-Q-72	2012-07-06	GN-2012B-Q-109
ULAS J0349–00			2012-10-09	GN-2012B-Q-109
ULAS J0815+24	2013-01-13,15	GS-2012B-Q-72	2011-02-06	GN-2011A-Q-59
ULAS J0838+24			2011-01-25	GN-2011A-Q-59
ULAS J0916+30			2011-01-25	GN-2011A-Q-59
ULAS J1240+25W	2012-12-19	GN-2012B-Q-109	2013-01-16	GN-2012B-Q-109
ULAS J1240+25E	2012-12-18	GN-2012B-Q-109	2013-01-16	GN-2012B-Q-109
ULAS J1409+07	2011-05-13	GS-2011A-Q-90		
ULAS J1607+26	2011-05-01	GN-2011A-Q-98		
ULAS J1640+28	2011-07-21	GN-2011A-Q-98	2011-02-02	GN-2011A-Q-59
SDSS J2153+45	2011-07-04	GN-2011A-Q-98		
ULAS J2206+02	2012-09-12,15	GS-2012B-Q-72		
ULAS J2315–00	2012-10-11	GN-2012B-Q-109	2012-07-18	GN-2012B-Q-109
ULAS J2330+05	2012-07-26	GS-2012B-Q-72	2012-07-10	GN-2012B-Q-109

^aOptical spectrum available in SDSS.

Table 4. NIRI Photometry for LAS White Dwarf Candidates

Short Name	$Y(\text{err})$	$J(\text{err})$	$H(\text{err})$	$K(\text{err})$
ULAS J0024–00	...	18.85(0.03)	18.58(0.03)	18.47(0.04)
ULAS J0100+11	18.44(0.03)	18.31(0.04)
ULAS J0156–00	19.74(0.05)	19.50(0.04)	18.93(0.04)	18.83(0.04)
ULAS J0349–00	19.80(0.05)	19.65(0.04)	19.05(0.04)	18.99(0.05)
ULAS J0815+24	18.45(0.04)	18.26(0.04)
ULAS J0838+24	19.15(0.03)	19.18(0.03)
ULAS J0916+30	19.15(0.04)	18.72(0.07)
ULAS J1240+25W	19.28(0.03)	18.98(0.02)	18.69(0.02)	18.55(0.04)
ULAS J1240+25E	19.08(0.03)	18.86(0.02)	18.59(0.02)	18.44(0.04)
ULAS J1640+28	...	19.69(0.04)	19.41(0.07)	...
ULAS J2315–00	18.59(0.05)	18.39(0.04)
ULAS J2330+05	18.20(0.03)	18.10(0.03)

Note. — Photometry is on the Mauna Kea Observatories (Vega) system (Tokunaga & Vacca 2005).

Table 5. CO5BOLD Simulations of Very Cool Pure-H DC White Dwarfs

Dim.	T_{eff} (K)	$\log g$ [cgs]	time (s)	$t_{\text{adv}} (\tau_{\text{R}} = 1)$ (s)	$t_{\text{rad}} (\tau_{\text{R}} = 1)$ (s)	$H_{\text{p}} (\tau_{\text{R}} = 1)$ (m)	Char. size (m)	Mach ($\tau_{\text{R}} = 1$)
2D	3770	8.0	1000	—	—	—	—	—
3D	3770	8.0	10	0.3	260	17	69	0.02
2D	4520	8.0	1000	—	—	—	—	—
3D	4520	8.0	10	0.1	60	22	78	0.03

Note. — All quantities were averaged over 250 snapshots and, when appropriate, on the constant geometrical depth that corresponds to $\langle \tau_{\text{R}} \rangle_z = 1$. T_{eff} is derived from the temporal and spatial average of the emergent flux, time is the total simulation time, t_{adv} the advective or turnover timescale, t_{rad} the radiative relaxation timescale, H_{p} the pressure scale height, and Char. size the characteristic horizontal size of the granulation. All quantities are defined in Tremblay et al. (2013b).

Table 6. Derived Properties of the LAS Sample

Short Name	Spectral Type	Composition	T_{eff} (K)	$T_{\text{H}\alpha}$ (K)	Cool. Age (Gyr)	Distance (pc)	v_{tan} (km s ⁻¹)
ULAS J0024–00	DC	Unconstrained	4610 ± 130	—	7.1 ^{+2.3} _{-3.5}	98 ± 21	78 ± 17
ULAS J0049–00	DA	H	6290 ± 90	5700	2.0 ^{+1.8} _{-0.6}	141 ± 26	83 ± 15
ULAS J0100+11	—	He	4140 ± 80	—	8.0 ^{+0.2} _{-3.0}	88 ± 19	49 ± 11
ULAS J0121–00	DC	H	4320 ± 100	—	8.2 ^{+1.6} _{-2.8}	71 ± 10	33 ± 5
ULAS J0142+00	DA	H	6010 ± 100	5650	2.2 ^{+2.0} _{-0.7}	149 ± 27	74 ± 13
ULAS J0226–00	DA	H	5620 ± 120	5550	2.8 ^{+2.4} _{-1.1}	157 ± 28	82 ± 15
ULAS J0302+00	DC	He	5630 ± 150	—	3.5 ^{+2.2} _{-1.5}	171 ± 34	99 ± 20
ULAS J0815+24	DC	H	4150 ± 100	—	8.6 ^{+1.4} _{-2.7}	72 ± 11	42 ± 7
ULAS J0826–00	DC	H	4100 ± 130	—	8.8 ^{+1.3} _{-2.6}	76 ± 9	33 ± 4
ULAS J0840+05	DC	Mixed	4360 ± 140	—	7.5 ^{+0.4} _{-3.0}	82 ± 16	44 ± 9
ULAS J0916+30	—	Unconstrained	5630 ± 240	—	3.3 ^{+2.7} _{-1.6}	168 ± 42	58 ± 15
ULAS J1006+09	DC	He	4250 ± 110	—	7.8 ^{+0.4} _{-3.2}	72 ± 17	50 ± 12
ULAS J1206+03	DC	He	4570 ± 70	—	7.0 ^{+0.7} _{-2.2}	92 ± 19	72 ± 15
ULAS J1240+25E	DA	H	5570 ± 50	5250	3.0 ^{+2.6} _{-1.2}	130 ± 25	163 ± 31
ULAS J1240+25W	DA?	H	5130 ± 50	—	5.0 ^{+2.8} _{-2.5}	124 ± 24	154 ± 30
ULAS J1320+08	DC	Mixed	4810 ± 130	—	6.5 ^{+0.8} _{-3.1}	103 ± 19	96 ± 18
ULAS J1323+12	DA	H	5270 ± 70	5300	4.3 ^{+2.8} _{-2.1}	107 ± 19	106 ± 19
ULAS J1345+15	DC	H	3990 ± 80	—	9.0 ^{+1.4} _{-2.7}	57 ± 9	71 ± 11
ULAS J1351+12	DC	He	4780 ± 60	—	6.5 ^{+0.9} _{-3.2}	101 ± 20	58 ± 12
ULAS J1404+13	DC	Mixed	4350 ± 140	—	7.5 ^{+0.4} _{-2.7}	59 ± 9	43 ± 7
ULAS J1409+07	DC	H	4710 ± 30	—	6.9 ^{+2.1} _{-3.2}	60 ± 11	64 ± 12
ULAS J1436+05	DC	Unconstrained	4320 ± 170	—	7.9 ^{+2.1} _{-3.7}	56 ± 13	84 ± 19
ULAS J1454–01	DC	Unconstrained	4700 ± 80	—	6.8 ^{+2.4} _{-3.4}	63 ± 13	63 ± 13
ULAS J1522+08	DA	H	5370 ± 130	5450	3.7 ^{+2.9} _{-1.7}	151 ± 28	75 ± 14
ULAS J1607+26	DC	H	4450 ± 50	—	7.7 ^{+1.9} _{-3.3}	64 ± 12	49 ± 9
ULAS J2206+02	DC	H	4120 ± 70	—	8.7 ^{+1.6} _{-2.9}	58 ± 10	58 ± 10
ULAS J2330+05	DC	Unconstrained	4465 ± 380	—	7.6 ^{+2.4} _{-4.1}	74 ± 23	61 ± 19
ULAS J2331–00	DA	H	6310 ± 130	5550	2.0 ^{+1.8} _{-0.6}	183 ± 34	119 ± 22
ULAS J2331+15	DA	H	5030 ± 60	5100	5.5 ^{+0.9} _{-2.8}	99 ± 20	75 ± 15
ULAS J2339–00	DA	H	6450 ± 200	5900	1.9 ^{+1.7} _{-0.6}	189 ± 35	92 ± 17

Note. — We assume $\log g = 8$ and uncertainties are computed from the photometric scatter and an allowed range in gravity of $7.7 \leq \log g \leq 8.3$. The tangential velocity is calculated from the distance and proper motion given in Table 1 and Paper I and II. For J1323+12 we rely on the alternative proper motion given in Paper II. We do not include ULAS J1528+06 and J1554+08 from Paper I which were found to be subdwarfs. We also exclude LAS white dwarfs that were previously discovered in the SDSS (SDSS J2242+00; Kilic et al. 2006, and SDSS J1247+06; Kilic et al. 2010).

Table 7. Fraction of Helium Dominated Atmospheres

T_{eff} range (K)	LAS sample (this work)	Giammichele et al. 2012 ^a	Kilic et al. 2009	Kilic et al. 2010
$7000 < T_{\text{eff}} < 8000$	—	53%	—	—
$6000 < T_{\text{eff}} < 7000$	—	50%	—	—
$5000 < T_{\text{eff}} < 6000$	25%	25%	11%	30% ^b
$4000 < T_{\text{eff}} < 5000$	46% ^c	24%	4%	14-59% ^d

Note. — Helium dominated atmospheres are defined as DC, DZ, or DQpec with $\text{He}/\text{H} > 1$. For completeness, we include the two SDSS white dwarfs re-discovered in the LAS sample (see notes in Table 6).

^aWe only include objects within 20 pc.

^bWe only include objects with a spectroscopic confirmation of the spectral type.

^cWe do not include the two objects unconfirmed as white dwarfs as well as the unconstrained compositions.

^dThe lower limit considers that all DC white dwarfs with derived pure-He atmospheres are actually pure-H atmospheres.

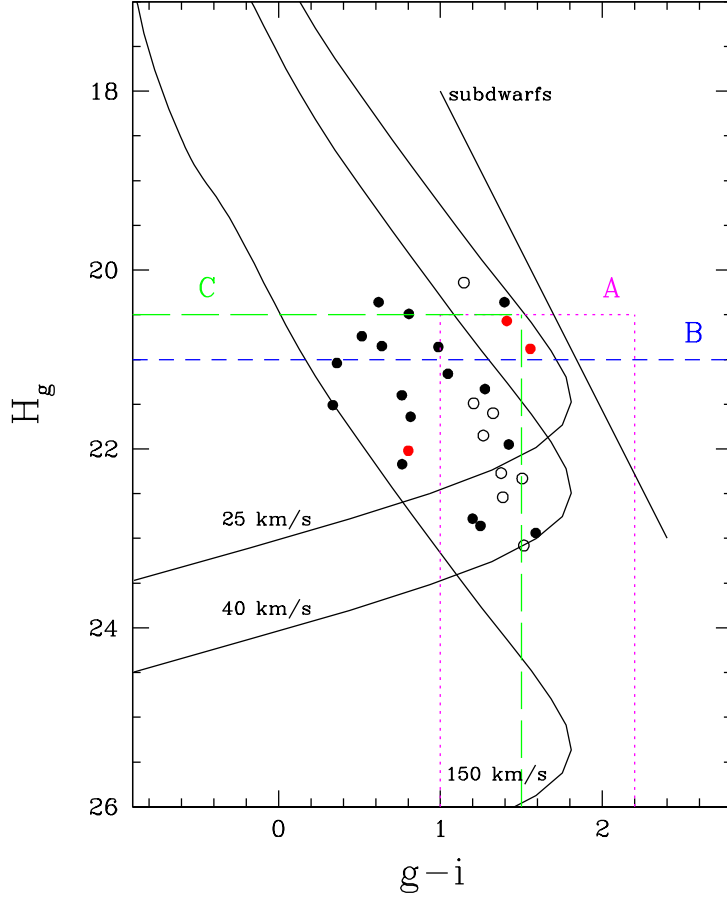


Fig. 1.— Reduced g -band proper motion as a function of $g - i$. We display the published sample of Paper I and II (filled circles) and the white dwarfs discovered in this work (open circles). Mixed He/H objects are identified in red. White dwarf cooling curves (solid lines) for $v_{\text{tan}} = 25$ and 40 km s^{-1} represent the thin disk population, and the $v_{\text{tan}} = 150 \text{ km s}^{-1}$ track illustrates the position of halo white dwarfs. The estimated empirical location of subdwarfs is also shown based on Kilic et al. (2010). The regions labeled as A (dotted), B (short dashed), and C (long dashed) indicate the search criteria (see Table 1).

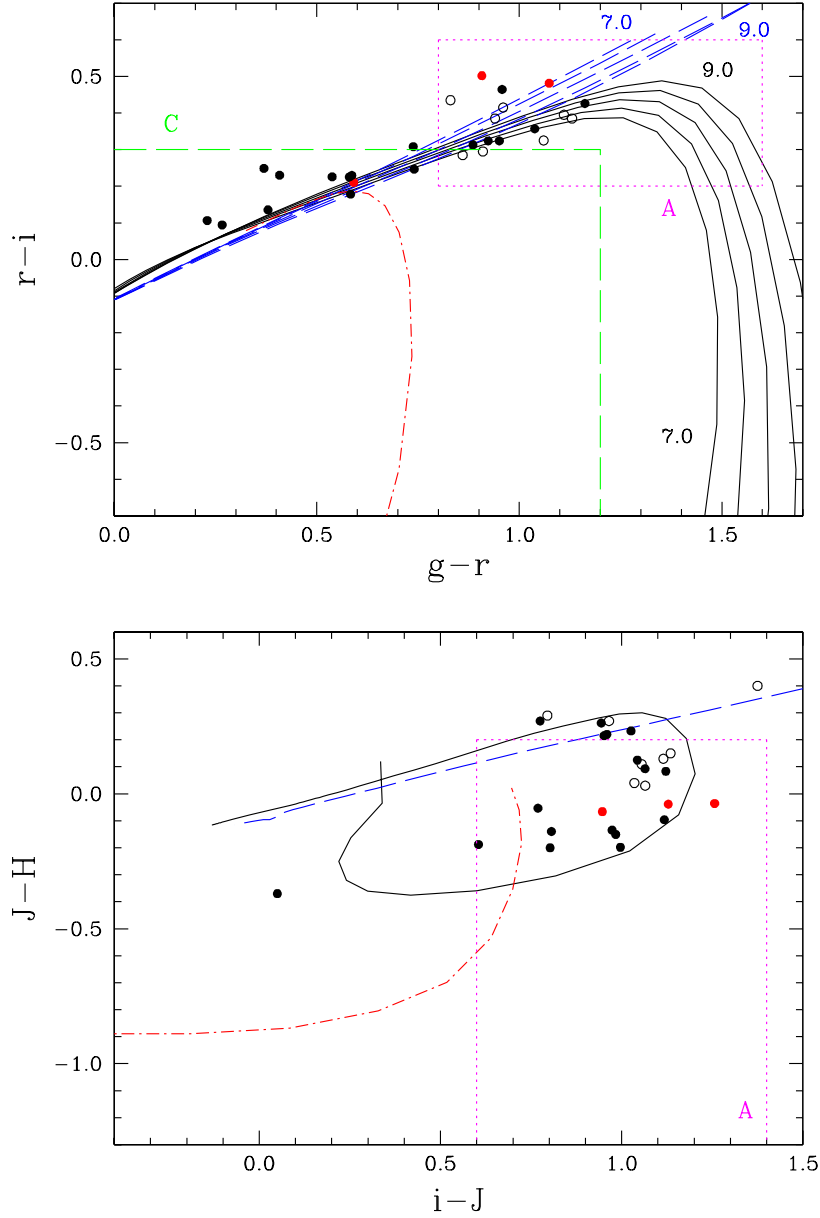


Fig. 2.— $r-i$ vs. $g-r$ (top) and $J-H$ vs. $i-J$ (bottom) color vs. color diagrams showing the color selection of white dwarf candidates. Model sequences at $\log g = 8$ are traced for pure-H atmospheres (solid, black), pure-He atmospheres (dashed, blue), and mixed He/H = 100 atmospheres (dot-dashed, red). On the top panel we also display pure-H and pure-He sequences from $\log g = 7.0$ to 9.0 with steps of 0.5 dex (extreme values are identified on the panel). We show the published sample of Paper I and II (filled circles) and the new white dwarfs identified in this work (open circles). Mixed He/H objects are identified in red. The regions labeled A (dotted, magenta) and C (dashed, green) indicate the search criteria (see Table 1). The search region B covers the full range shown in the panels and search query C does not apply for objects with H detection.

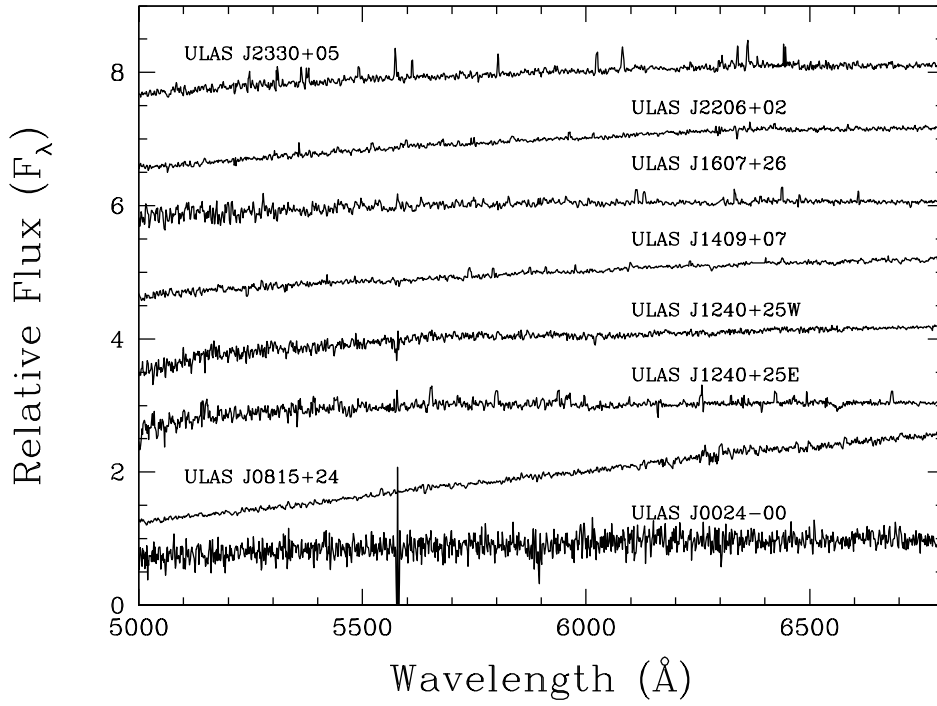


Fig. 3.— GMOS spectra of white dwarfs identified in the LAS DR9. We have no spectroscopic observations for J0100+11 and J0916+30. The spectra have been normalized to unity at 6000 Å and offset in steps of one flux unit for clarity.

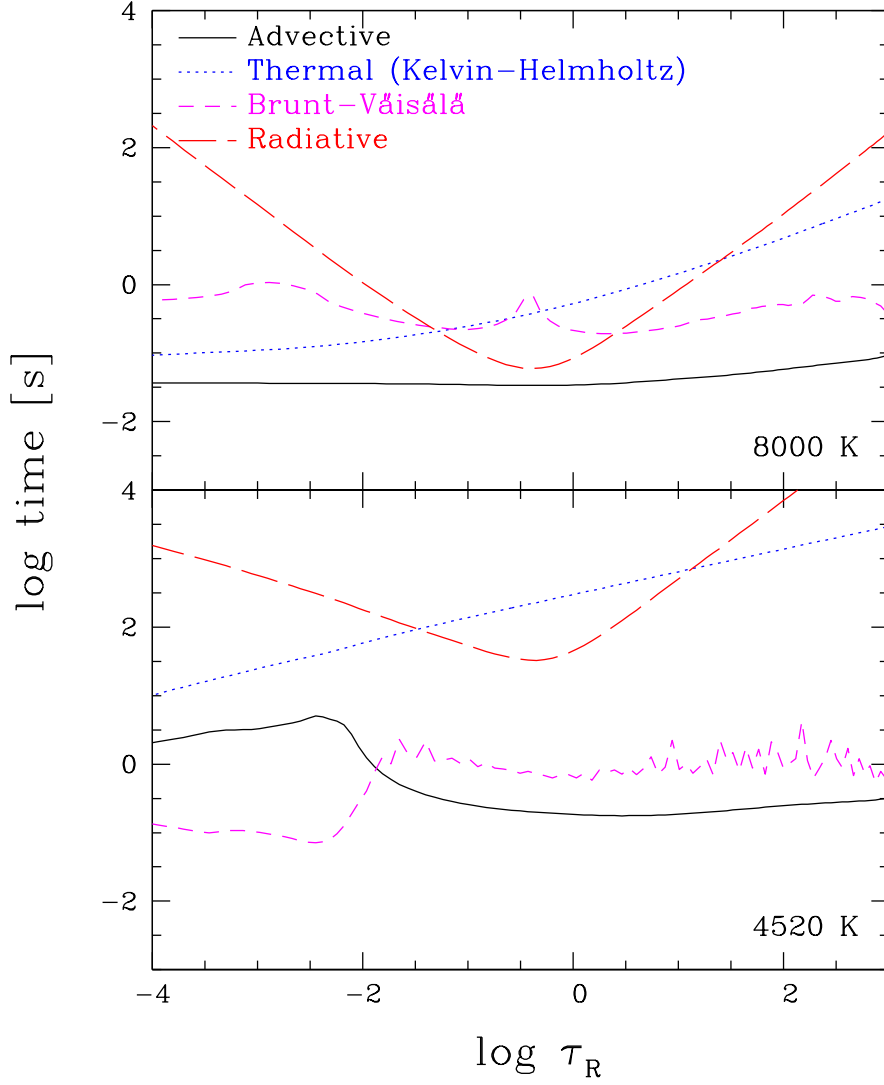


Fig. 4.— Timescales for the mean 3D structure of a 8000 (top panel) and 4520 K (bottom panel) pure-H white dwarf ($\log g = 8$) as a function of $\log \tau_R$. The different timescales are identified in the legend, and correspond to the advective timescale (black, solid), the Kelvin-Helmholtz timescale (blue, dotted), the Brunt-Väisälä timescale (cyan, short dashed) and the radiative timescale (red, long dashed). See Tremblay et al. (2013a, Eq. 1-4) for the timescale definitions. Features at small optical depth ($\log \tau_R < -2$) in the Brunt-Väisälä and advective timescales are likely numerical.

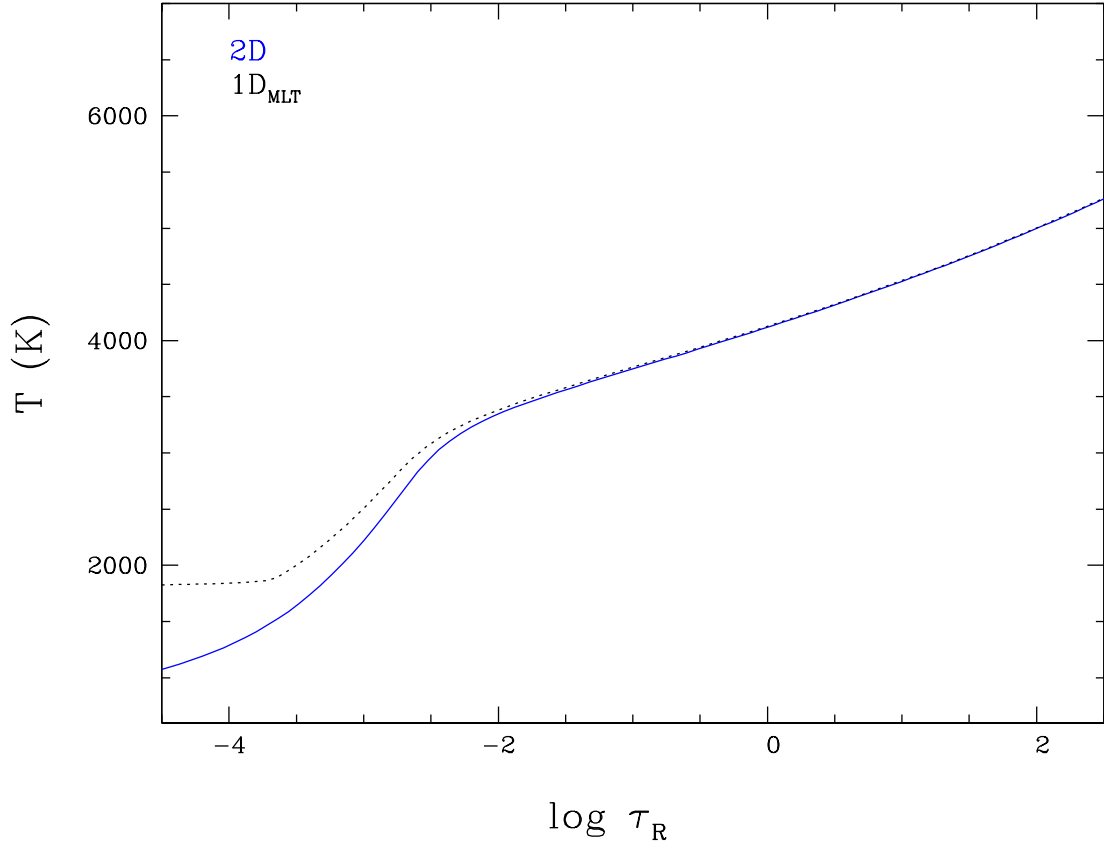


Fig. 5.— Non-gray temperature structure for a pure-H atmosphere at 3770 K and $\log g = 8$ from 2D (blue, solid) and 1D (black, dotted) models.

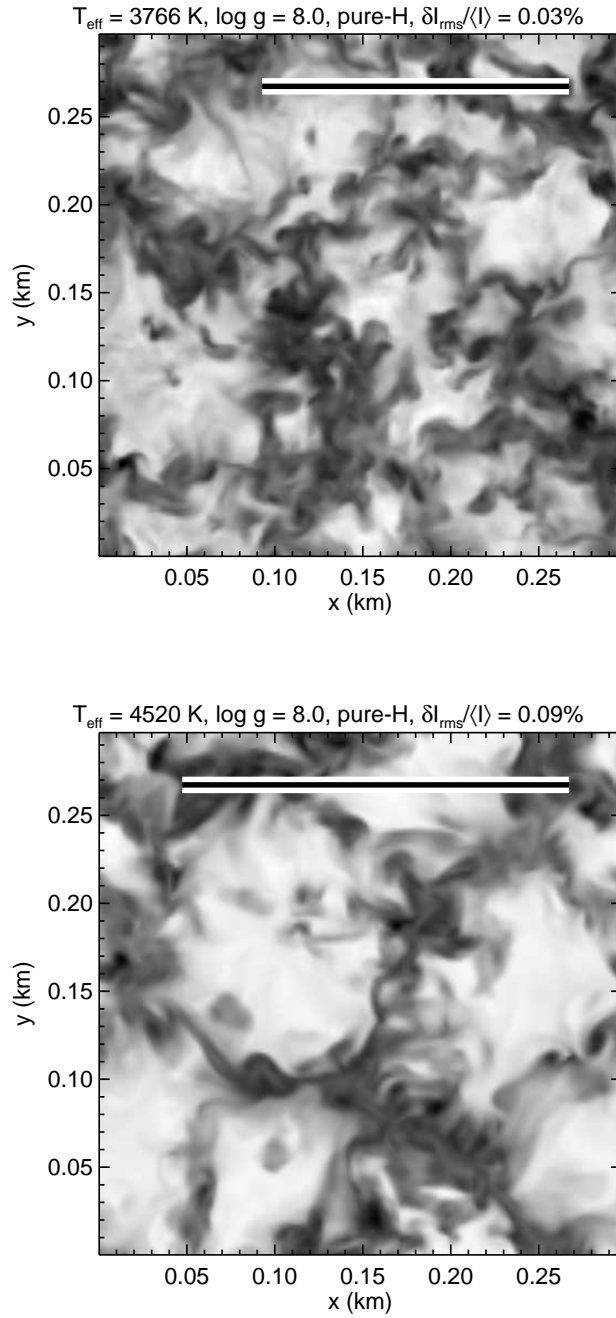


Fig. 6.— Emergent bolometric intensity at the top of the horizontal xy plane of the 3D white dwarf simulations at $T_{\text{eff}} = 3766 \text{ K}$ (*top*), 4520 K (*bottom*), and $\log g = 8$. The root-mean-square intensity contrast with respect to the mean intensity ($\delta I_{\text{rms}}/I$) is identified above the panels. The length of the bar in the top right is ten times the pressure scale height at $\tau_{\text{R}} = 1$.

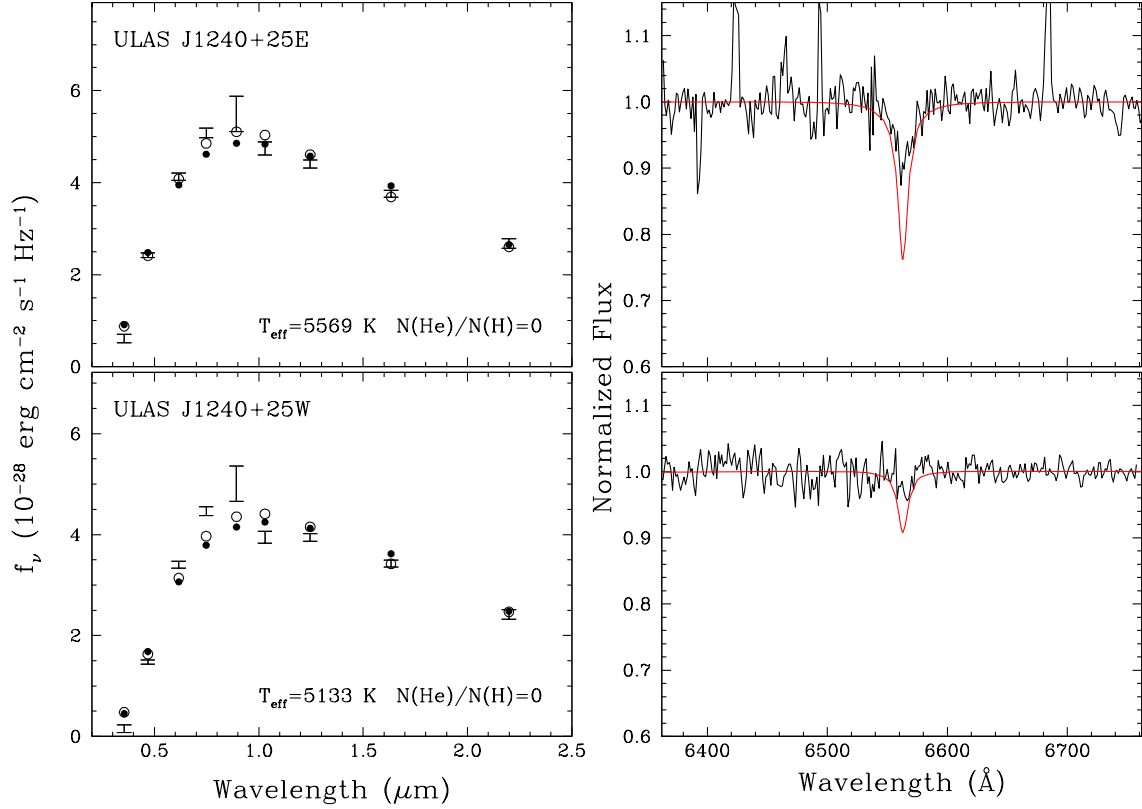


Fig. 7.— *Left panels:* Fit of the two components of a resolved white dwarf binary system from the LAS DR9 sample. The error bars in the left panels represent SDSS ugriz and LAS YJHK photometry. The best fit models, averaged over the filter bandpasses, are shown for pure-H (filled circles) and pure-He compositions (open circles). A surface gravity of $\log g = 8$ is assumed, and the derived T_{eff} is shown in the legends for the selected composition. *Right panels:* Observed spectra around $\text{H}\alpha$, with the modeled pure-H atmosphere line profiles based on the atmospheric parameters derived from photometry (solid red line). The detection of $\text{H}\alpha$ in J1240+25W is uncertain.

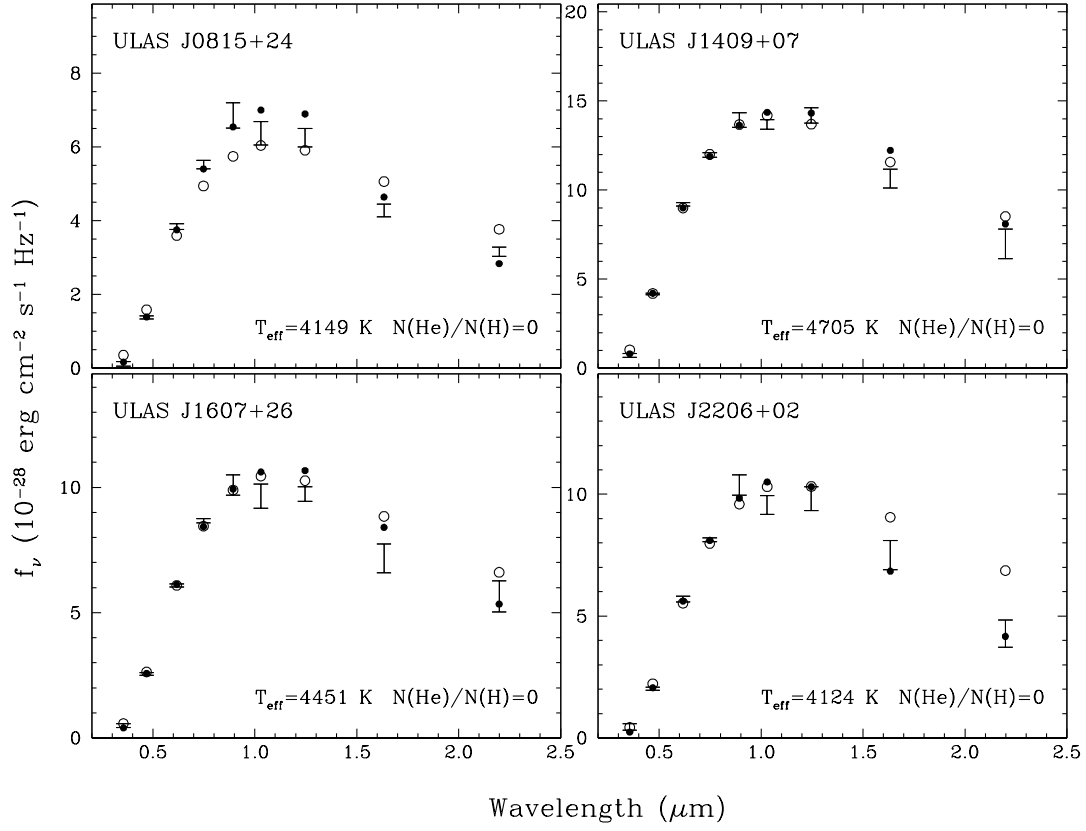


Fig. 8.— Four white dwarfs from the LAS DR9 sample best fit with pure-H atmospheres. Symbols are as in Figure 7. All objects have observed and modeled featureless spectra (not shown).

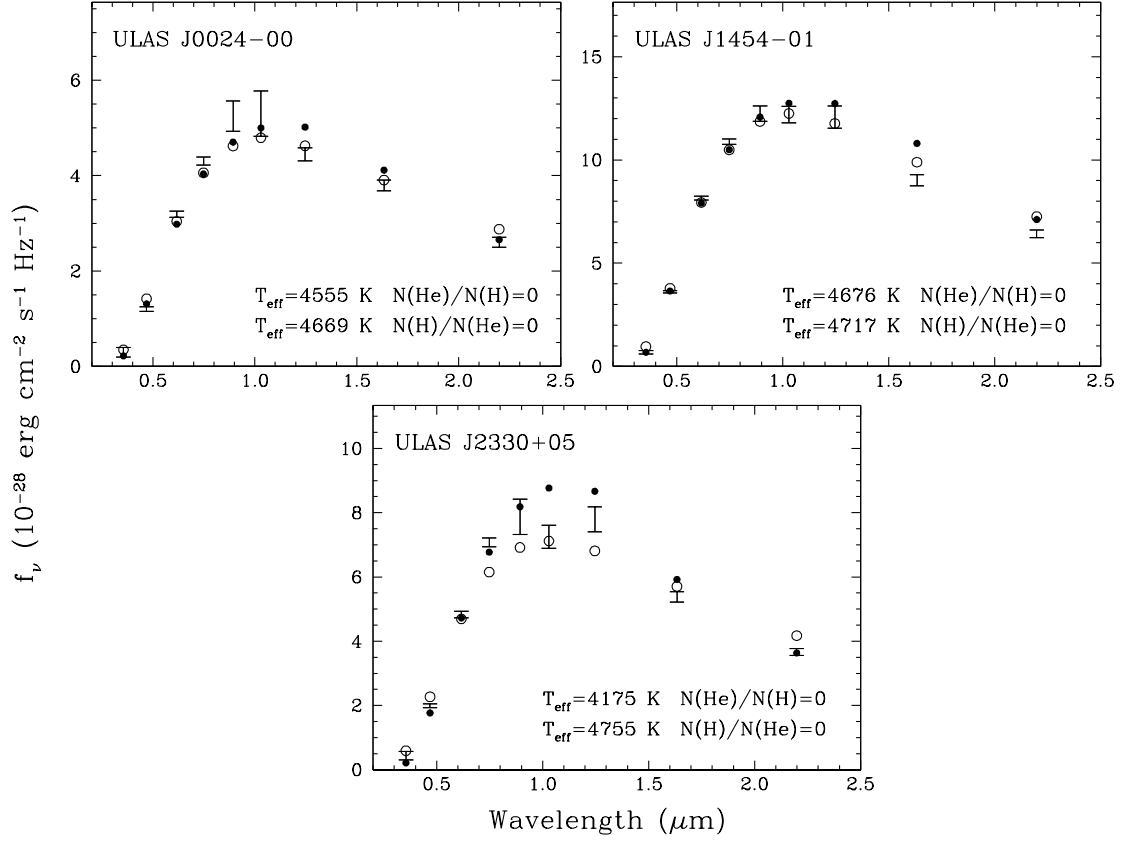


Fig. 9.— White dwarfs in the LAS DR9 sample and from Leggett et al. (2011, J1454-01) with an unconstrained composition. Symbols are the same as in Figure 7 and we show the derived T_{eff} for both compositions in the legends. The observed and modeled spectra are featureless.

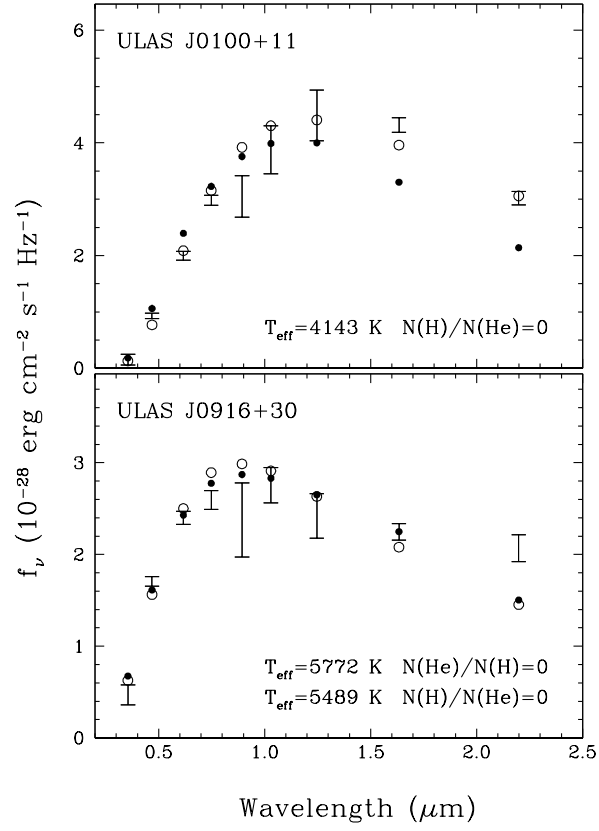


Fig. 10.— Two white dwarf candidates in the LAS DR9 sample with no spectroscopic observations. J0916+30 has an unconstrained composition. Symbols are the same as in Figure 9.

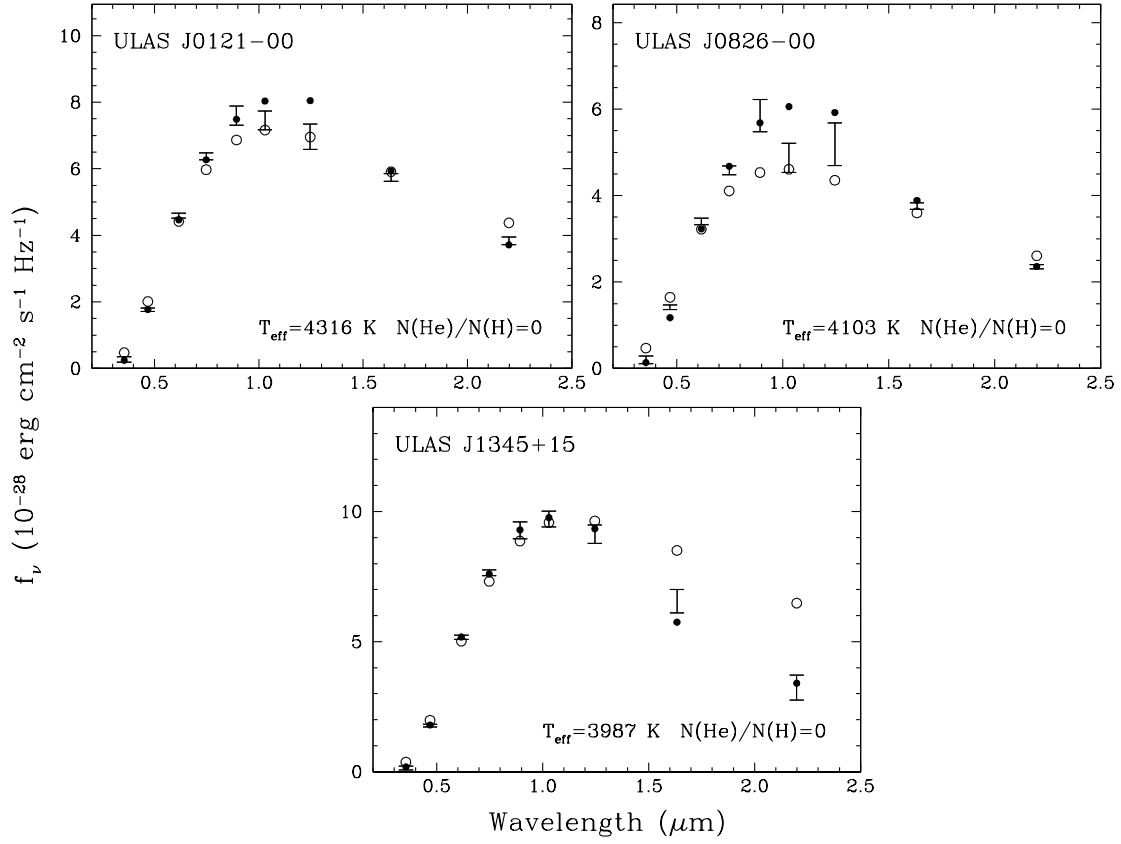


Fig. 11.— Improved fits for three objects from the Leggett et al. (2011) sample with pure-H models (filled circles) including the $\text{Ly}\alpha$ opacity (Kowalski & Saumon 2006). The derived T_{eff} is shown in the legends and we also display the pure-He composition best fit (open circles).

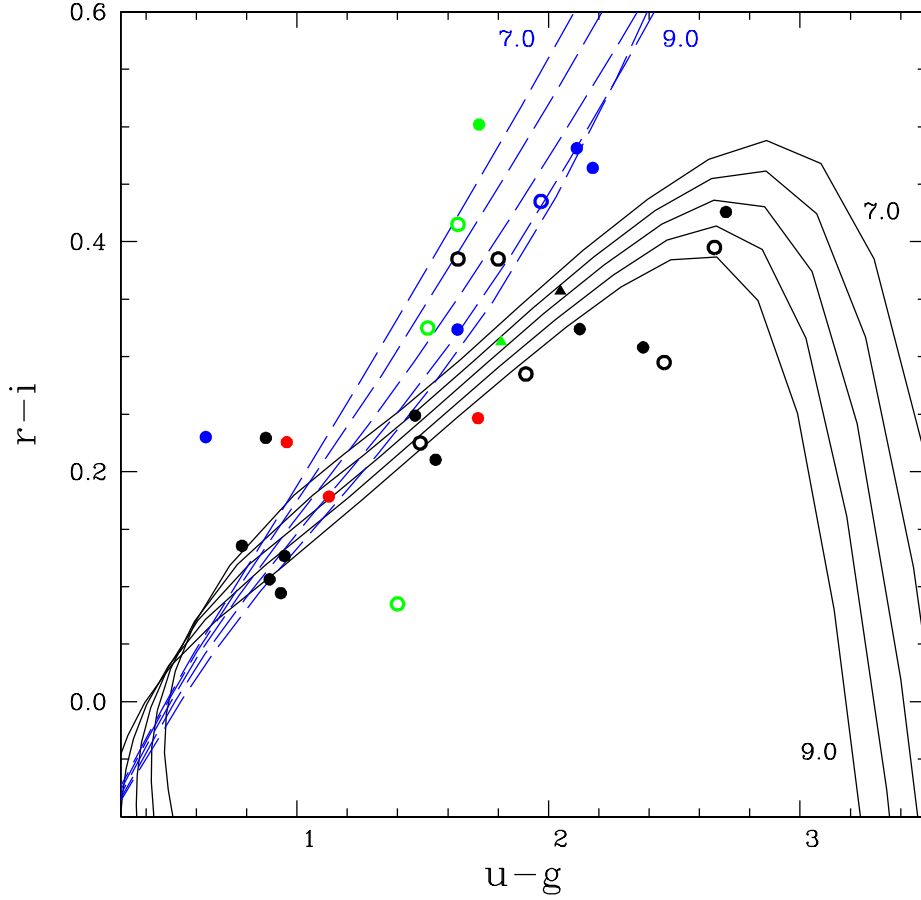


Fig. 12.— $r-i$ vs. $u-g$ color vs. color diagram for white dwarfs in the ULAS sample with a derived pure-H (black), pure-He (blue), mixed (red), or unconstrained (green) composition. The new white dwarfs identified in this work are shown with open circles while objects identified in Paper I and II are identified by filled circles when the derived composition is unchanged, or with filled triangles in the two cases where we have updated the composition. Theoretical color sequences for pure-H (solid, black) and pure-He atmospheres (dashed, blue) are also shown for $\log g = 7.0, 7.5, 8.0, 8.5$, and 9.0 (extreme values are identified on the panel).

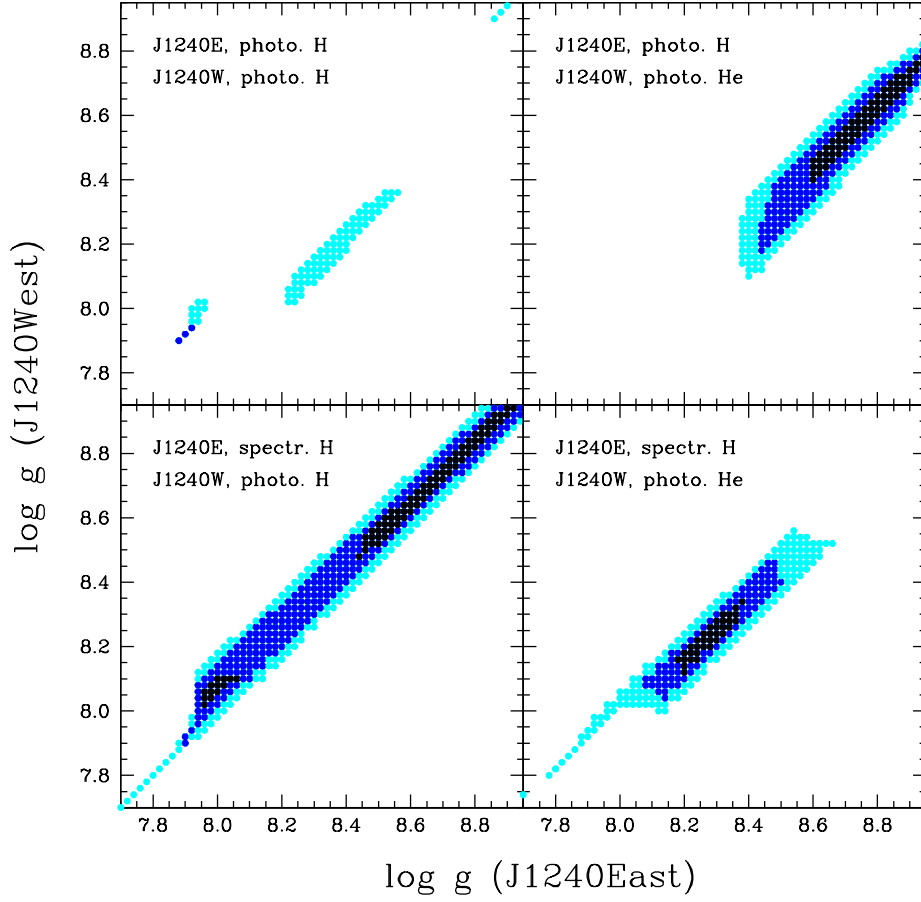


Fig. 13.— The $\log g$ couples for J1240+25E and J1240+25W where both the ages and distances are in agreement are shown when accounting for 1σ (black circles), 2σ (blue), and 3σ (cyan) of the photometric variance. The separate panels illustrate different assumptions about atmospheric parameters. We rely on the photometric and spectroscopic T_{eff} for J1240+25E on the top and bottom panels, respectively. J1240+25W is assumed to have pure-H and pure-He compositions on the left and right panels, respectively.

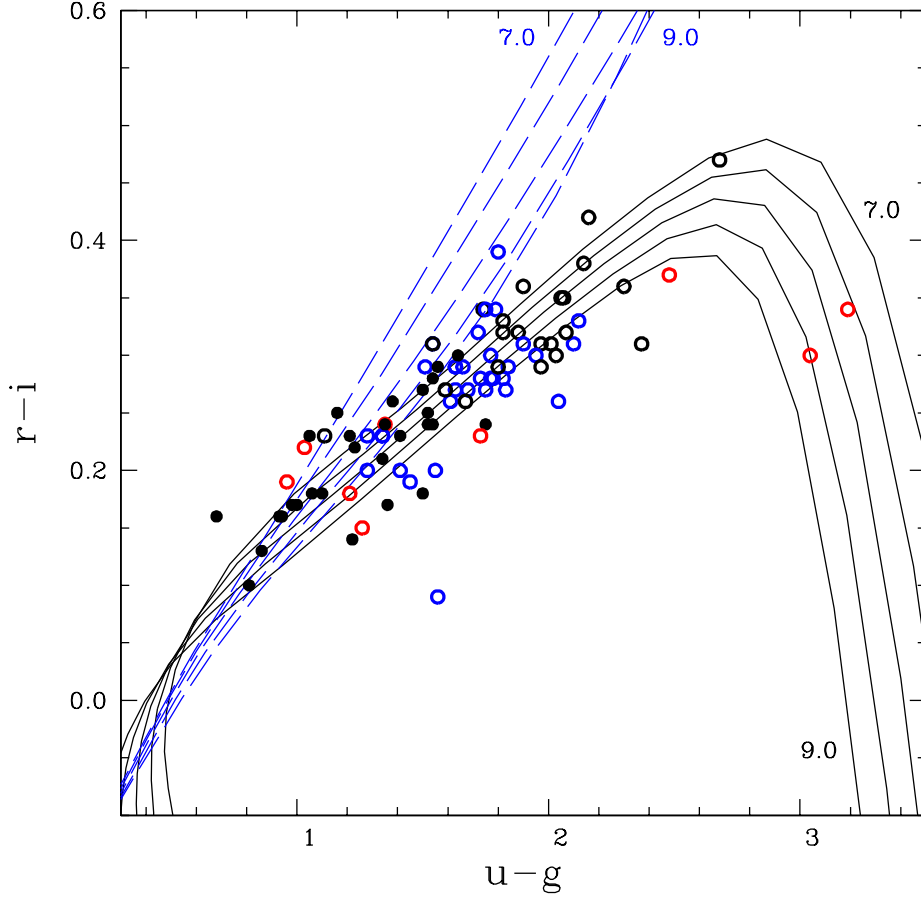


Fig. 14.— Similar to Figure 12 but for white dwarfs identified in the Kilic et al. (2010) sample. We only include objects with a DA (filled circles) or DC (open circles) spectroscopic classification. We also identify the objects for which Kilic et al. derived pure-H (black), pure-He (blue), and mixed (red) compositions. These classifications are with model atmospheres not including the $\text{Ly}\alpha$ red-wing opacity.